The Astrophysical Journal, 627:346–367, 2005 July 1

AFTERGLOW EMISSION FROM PAIR-LOADED BLAST WAVES IN GAMMA-RAY BURSTS

Andrei M. Beloborodov[1]
Physics Department and Columbia Astrophysics Laboratory, Columbia University, 538 West 120th Street, New York, NY 10027
Received 2004 November 18; accepted 2005 March 3

ABSTRACT

The MeV radiation front of gamma-ray bursts creates copious $e^{\pm}$ pairs as it propagates through an ambient medium. The created pairs enrich the leptonic component of the medium by a large factor at distances $R < R_{\rm load} \sim 10^{16}$ cm from the burst center. The following blast wave sweeps up the pair-rich medium and then emits the observed afterglow radiation. We find that the afterglow has a "memory" of $e^{\pm}$ loading outside $R_{\rm load}$. The $e^{\pm}$ remain in the swept-up material and slowly cool down by emitting synchrotron radiation. They are likely to dominate the blast wave emission in IR, optical, and UV bands during the first minutes of the observed afterglow. The $e^{\pm}$ afterglow is described by a simple formula, which is derived analytically and checked by numerical integration of synchrotron emission over the blast material; a suitable Lagrangian formalism is developed for such calculations. The main signature of $e^{\pm}$ radiation is its flat ("white") spectrum in a broad range of frequencies from IR to UV and possibly soft X-rays. This radiation can be detected by the *Swift* satellite, which would enable new observational tests for the explosion physics.

Subject headings: cosmology: miscellaneous — gamma rays: bursts — radiation mechanisms: nonthermal — shock waves

Online material: color figures

1. INTRODUCTION

Cosmological gamma-ray bursts (GRBs) are produced by powerful explosions in distant galaxies. It is not yet clear how the explosion is triggered; however, its basic phenomenological picture has been established: an ultrarelativistic shell ("fireball") is ejected by a compact central engine. The expanding shell emits the burst of γ-rays, then sweeps up an ambient medium, and decelerates, producing the observed afterglow radiation. The afterglow is explained as synchrotron emission of nonthermal electrons in the relativistic blast wave (for a recent review see Piran 2004).

Thompson & Madau (2000) pointed out that an external medium must be $e^{\pm}$ loaded and preaccelerated by the leading γ-ray front (prompt GRB radiation), which should affect the ensuing shock wave. The effect is a result of γ-ray transfer through the optically thin medium (Beloborodov 2002, hereafter B02), which involves a runaway of pair creation. A tiny fraction of GRB radiation participates in this transfer; however, it impacts dramatically the circumburst medium. The transfer problem was solved in B02, and the number of loaded $e^{\pm}$ and the Lorentz factor of the medium behind the γ-ray front were calculated. The loaded pairs were found to dominate the ambient medium at radii $R < R_{\rm load} \approx 1.6\times10^{16}(E_\gamma/10^{53}$ ergs) cm, where E_γ is the isotropic (4π) equivalent of the GRB energy.

The $e^{\pm}$ loading sets the stage for the immediately following shock wave driven by the GRB ejecta. The shock heats and accelerates the particles of the medium, and a nonthermal $e^{\pm}$ population is expected to form behind the shock front, which produces synchrotron radiation. The goal of the present paper is to calculate emission from the pair-loaded postshock plasma in the expanding blast wave.

This complicated problem was previously approached in a few works. B02 evaluated the shock parameters at $R < R_{\rm load}$ and found that the GRB afterglow should start with a brief and bright optical signal; however, B02 did not calculate the expected light curve or spectrum of $e^{\pm}$ radiation. Then Li et al. (2003) calculated the light curve considering the blast wave as a single shell with an averaged $e^{\pm}$ density and a common electron spectrum. This is not a good approximation as discussed in detail below. In particular, at $R > R_{\rm load}$, only a small fraction of the blast wave material is dominated by pairs, and its emission dramatically differs from the rest of swept-up material.

Most recently, Kumar & Panaitescu (2004) studied $e^{\pm}$-loaded blast waves. They focused on GRBs where the γ-ray front only partially overtakes the shock wave at $R_{\rm load}$. A new effect appears in that situation, which was neglected in Kumar & Panaitescu (2004): the postshock $e^{\pm}$ overlap with the γ-ray front and are exposed to 0.1–1 MeV photons (keV in the plasma frame); therefore $e^{\pm}$ are quickly cooled by inverse Compton scattering. Most of the $e^{\pm}$ energy is then emitted by upscattering 0.1–1 MeV photons to GeV–TeV band, and their optical synchrotron emission is suppressed (Beloborodov 2005).

Whether the γ-ray front still overlaps with the blast wave at a radius of interest depends on the front thickness (proportional to the duration of the prompt GRB) and the blast wave Lorentz factor Γ.[2] So, two qualitatively different regimes of early afterglows are possible:

1. "Long-burst" (or "thick-shell") regime where the prompt GRB radiation overlaps the early blast wave. Then a strong GeV–TeV flash should be produced, and the early optical emission is suppressed.
2. "Short-burst" (or "thin-shell") regime where the prompt γ-rays early overtake the external shock wave, and $e^{\pm}$ creation

[1] Also at Astro-Space Center, Lebedev Physical Institute, Profsojuznaja 84/32, Moscow 117810, Russia.

[2] The γ-ray front can be emitted when the explosion has a small radius, well before the blast wave forms; however, they may still overlap at large radii because the ejecta expands with almost the speed of light. The γ-ray front is faster by a small $\delta v = c/2\Gamma^2 \sim 10^{-5}c$ and completely overtakes the relativistic blast wave at time $R/c \gtrsim \Delta/\delta v$.

and Compton cooling take place *ahead* of the shock. Then the postshock plasma is not exposed to the prompt radiation and not Compton cooled. A bright optical emission can be expected in this situation.

In the present paper we focus on the short-burst regime. GRBs that satisfy this condition have short durations t_b and/or modest Lorentz factors of the blast wave Γ (B02),

$$t_b < 10\left(\frac{\Gamma}{100}\right)^{-2}\left(\frac{R_{\rm acc}}{10^{16}\ {\rm cm}}\right)\frac{(1+z)}{2}\ {\rm s}, \qquad (1)$$

where $R_{\rm acc} = 5^{-1/2}R_{\rm load}$ is a characteristic radius where most of the optical-emitting pairs are created and z is the cosmological redshift of the burst. We develop a suitable Lagrangian formalism that describes the synchrotron emission of pair-loaded blast waves and calculate the expected light curve and spectrum of the early afterglow. We find two distinct emission components produced at $R > R_{\rm load}$: (1) the relict $e^{\pm}$ component dominating the early emission from IR to soft X-rays, and (2) the recently shocked pair-free component that gives a standard afterglow emission initially peaking in X-rays and later evolving to softer bands.

In § 2 we briefly describe the pair creation process and the formation of blast wave in the pair-loaded medium behind the γ-ray front (details are found in B02). In § 3 we formulate the emission problem for $e^{\pm}$-loaded blast waves and develop their Lagrangian description. Numerically calculated examples of $e^{\pm}$-loaded afterglows are given in § 4.

In § 5 we show that the $e^{\pm}$ component of afterglow emission is described by a simple formula and practically independent of the details of the shock wave physics. The case of a uniform ambient medium is elaborated in § 6. In the present paper we focus on explosions in media of modest density $n_0 = 0.1$–$10^3\ {\rm cm}^{-3}$. Explosions in a high-density wind from a Wolf-Rayet progenitor will be considered in detail elsewhere. In that case, the $e^{\pm}$ loading has a much stronger effect on the afterglow emission (B02).

There are two shock fronts in a blast wave: forward and reverse. The reverse shock emits one more component of the early afterglow, which depends on the nature of the GRB ejecta. Differences between emissions from the reverse shock and the pair-loaded forward shock are discussed in § 7. The differences are significant and may allow one to distinguish observationally the two emission mechanisms when the *Swift* satellite provides the early afterglow data.

2. PAIR LOADING BY THE γ-RAY FRONT

A medium overtaken by a front of collimated γ-rays is inevitably $e^{\pm}$ loaded. This happens because some γ-rays Compton scatter off the medium and get absorbed by the primary collimated radiation via reaction $\gamma + \gamma \rightarrow e^+ + e^-$.

The medium is optically thin, so only a tiny fraction of the GRB radiation front scatters and turns into $e^{\pm}$; however, the number of created $e^{\pm}$ *per ambient electron* can be very large, $n_{\pm}/n_0 \gg 1$. The column density of an expanding photon front scales with radius as R^{-2}; hence, the number of scattered photons per ambient electron is decreasing as R^{-2} and $n_{\pm}/n_0 \gg 1$ at small R. The created $e^{\pm}$ do more scattering, which leads to an exponential runaway of pair creation. There is a sharp boundary $R_{\rm load}$ between the exponentially loaded $e^{\pm}$ region and the outer pair-free region. The pair creation and scattering of GRB radiation inside $R_{\rm load}$ are accompanied by momentum deposition and the medium is accelerated radially away from the center.

The pair-loading factor $n_{\pm}/n_0$ and acceleration of an optically thin medium in the γ-ray front do not depend on n_0 and can be calculated starting with just one ambient electron and one ambient proton to which the electron is coupled. The e and p components of the medium move always together to maintain neutrality of the plasma. Any momentum communicated to e is immediately shared with p, so that the effective mass of e is $m_e + m_p$. As the γ-ray front passes through, the electron component is enriched by a number of additional $e^{\pm}$ (then the mass per lepton is reduced) and altogether they acquire a Lorentz factor γ. This transformation is quick: it takes time $\sim(\Delta/c\gamma^2)$ in the fixed laboratory frame, during which the γ-ray front overtakes a given ambient electron.[3] The thickness of the γ-ray front Δ is related to the observed duration of the prompt GRB t_b by $t_b = (1+z)\Delta/c$.

A schematic explosion picture is shown in Figure 1. The radiation front leads the forward shock by a small distance[4]

$$l \approx \frac{R}{4\Gamma^2} \ll R \qquad (2)$$

and changes the ambient medium just before it is shocked. The medium ahead of the blast wave (but already overtaken by the γ-ray front) is described by the lepton number per ambient proton Z and Lorentz factor γ. The values $Z = 1$ and $\gamma = 1$ would correspond to a static pair-free medium.

The variables Z and γ are functions of only one parameter of the front, ξ, which we now define. Let dE_γ/dS be the energy column density of the γ-ray front (ergs per centimeter). The GRB is likely beamed, yet it is convenient to define its isotropic equivalent $E_\gamma = 4\pi R^2(dE_\gamma/dS)$. When an ambient electron is overtaken by the front, it scatters energy[5] $e_{\rm sc} = \sigma_{\rm T}(dE_\gamma/dS) = E_\gamma\sigma_{\rm T}/4\pi R^2$. The relevant dimensionless parameter is

$$\xi = \frac{e_{\rm sc}}{m_e c^2} = 65E_{\gamma,53}\,R_{16}^{-2}. \qquad (3)$$

The functions $Z(\xi)$ and $\gamma(\xi)$ were found numerically in B02. They are calculated by solving the radiative transfer problem coupled to the dynamic problem of the medium acceleration. We briefly summarize the calculations here.

Two processes play important roles in the γ-ray transfer: Compton scattering $\gamma + e^{\pm} \rightarrow \gamma_{\rm sc} + e^{\pm}$ and photon-photon absorption $\gamma_{\rm sc} + \gamma \rightarrow e^+ + e^-$ (here γ stands for a primary photon and $\gamma_{\rm sc}$ for a scattered photon). The same processes determine the deposited momentum and acceleration of the medium. The medium remains optically thin, so only single scattering is of interest, and the process $\gamma_{\rm sc} + e^{\pm} \rightarrow \gamma_{\rm sc} + e^{\pm}$ is negligible. Nevertheless, there is a nonlinearity in the problem because the scattering opacity of the medium is affected by $e^{\pm}$ creation and changes enormously across the front.

The problem would be simpler if the scattered photons instantaneously converted to $e^{\pm}$ (Thompson & Madau 2000; Mészáros et al. 2001); then there would be no need to solve the

[3] The velocity difference between the radiation front and the accelerated medium is $(1-\beta)c \approx c/2\gamma^2$.

[4] We assume that the shock wave is approximately adiabatic. Then $\Gamma_{\rm shock} \approx \sqrt{2}\Gamma$, where Γ is the Lorentz factor of the postshock material (which we hereafter call "blast" for brevity), and $l \approx R(1-\beta_{\rm shock}) = R/2\Gamma^2_{\rm shock} = R/4\Gamma^2$.

[5] Accurate calculation of scattering includes the Klein-Nishina correction to Thomson cross section $\sigma_{\rm T}$; however, in the definition of ξ, it is convenient to use $\sigma_{\rm T}$, which is independent of photon energy.

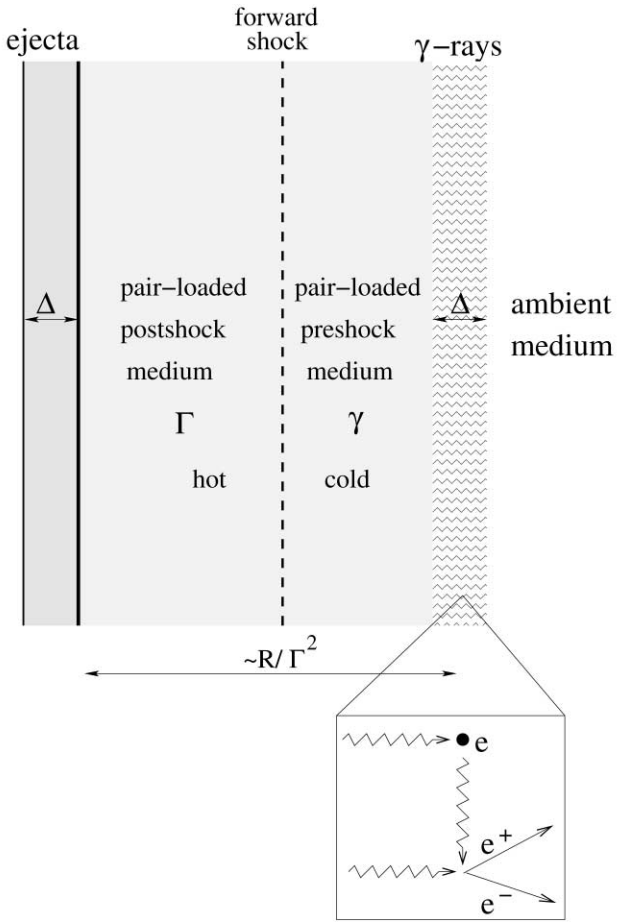

FIG. 1.—Early stage of a GRB blast wave ($R < R_{\rm load}$). The short-burst (or thin-shell) regime is assumed: $\Delta < R/4\Gamma^2$ (cf. eq. [1]). The forward shock propagates in the $e^{\pm}$-loaded and preaccelerated medium left behind the γ-ray front. The pair-loading factor Z and Lorentz factor γ of the preshock medium depend on the current radius R of the explosion (see Fig. 2). The inset schematically shows what happens in the γ-ray front: some of the γ-rays are scattered, lose their collimation, and get absorbed by the collimated γ-rays, producing $e^{\pm}$. The created pairs are immediately Compton cooled in the γ-ray front (B02), and the preshock medium is relatively cold ($kT < m_e c^2$). The pairs are heated/accelerated when the forward shock reaches them, and the postshock $e^{\pm}$ produce the broadband synchrotron emission. The whole structure—radiation front, $e^{\pm}$-loaded preshock medium, blast, and ejecta—has a small thickness $\sim R/\Gamma^2$.

radiative transfer. However, the bulk of scattered photons never convert to $e^{\pm}$ and escape. The formal absorption free path of a scattered photon in the radiation front turns out to be $\lambda_{\gamma\gamma} \gg \Delta$, which means that a scattered photon has a small chance $\Delta/\lambda_{\gamma\gamma}$ to create an $e^{\pm}$ pair. The exponential runaway of pair loading occurs when the smallness of this chance is compensated by a large number of scattered photons per electron, which requires a small scattering free path of the electron in the radiation front, $\lambda \ll \Delta$. The length of exponential $e^{\pm}$ loading is then $a = (\lambda\lambda_{\gamma\gamma})^{1/2} < \Delta$. The characteristic loading radius $R_{\rm load}$ is defined by $a = \Delta$; $\lambda \ll \Delta \ll \lambda_{\gamma\gamma}$ at this radius.

At small R, the $e^{\pm}$-loaded medium is accelerated to a significant Lorentz factor γ (not to be confused with the photon symbol γ in the reaction formulae). The photons scattered by the accelerating medium have the collimation angle $\delta\theta \approx \gamma^{-1}$, and their chances to convert to pairs become completely negligible. (A smaller angle between the scattered and primary photons implies a higher threshold for reaction $\gamma_{\rm sc} + \gamma \rightarrow e^+ + e^-$ and a smaller absorption opacity seen by the scattered photons.) Therefore, $e^{\pm}$ loading at small radii is made by photons scattered in a small leading portion of the front (where the medium has not yet acquired $\gamma \gg 1$) and propagated across the front.

The numerical solution to the transfer problem describes what exactly happens with the medium in the radiation front. The shell of ambient medium that is inside the front at a given moment of time has a certain velocity profile $\beta(\varpi)$ where $0 < \varpi < \Delta$ is the distance from the leading edge of the front ("entrance"). The medium velocity β increases from zero ($\gamma = 1$) at the entrance $\varpi = 0$ to its final value at the exit $\varpi = \Delta$. Lepton number per proton, Z, also increases from $Z = 1$ to its value behind the front. The front structure is described by the same functions $\gamma(\xi)$ and $Z(\xi)$ that describe the front evolution with radius if one substitutes $\xi = \varpi/\lambda$ (B02). So, the front structure is described by the same functions at different times; i.e., it is self-similar.

Since there is a gradient of the medium velocity inside the front (layers at larger ϖ move faster), one might think that caustics, i.e., internal shocks, can develop in the front. It never happens at radii of interest. The radiation overtaking the medium dictates its velocity, and the medium has no time to develop a caustic because it quickly exits the front[6] and is left behind with a uniform Lorentz factor γ (the exit γ gradually evolves on timescale $\sim R/c$ because $\xi = \Delta/\lambda$ evolves as R^{-2} as the front expands). The medium left behind the radiation front is immediately picked up by the blast wave, on a timescale $\sim (R/c)(\Gamma/\gamma)^2 \ll R/c$.

The exact numerical solution for $\gamma(\xi)$ and $Z(\xi)$ is well approximated by a simplified analytical model derived in B02 and summarized in the next section.

2.1. *Analytical Description of $e^{\pm}$ Loading*

The exact $Z(\xi)$ and $\gamma(\xi)$ are approximated by the following analytical formulae (see eqs. [49], [62], and [63] in B02; $Z = n^*/n_0$ in B02 notation):

$$Z(\xi) = \begin{cases} \dfrac{1}{2}\left[\exp\left(\dfrac{\xi}{\xi_{\rm load}}\right) + \exp\left(-\dfrac{\xi}{\xi_{\rm load}}\right)\right], & \xi < \xi_{\rm acc}, \\ \left(\dfrac{\xi}{\xi_{\rm acc}}\right)^2 Z_{\rm acc}, & \xi_{\rm acc} < \xi < 3\xi_{\rm acc}, \\ 3\left(\dfrac{\xi}{\xi_{\rm acc}}\right) Z_{\rm acc}, & \xi > 3\xi_{\rm acc}, \end{cases} \tag{4}$$

$$\gamma(\xi) = \begin{cases} 1, & \xi < \xi_{\rm acc}, \\ \left(\dfrac{\xi}{\xi_{\rm acc}}\right)^3, & \xi_{\rm acc} < \xi < 3\xi_{\rm acc}, \\ 3\sqrt{3}\left(\dfrac{\xi}{\xi_{\rm acc}}\right)^{3/2}, & \xi > 3\xi_{\rm acc}, \end{cases} \tag{5}$$

where $\xi_{\rm acc} = (5 + \ln \mu_e)\xi_{\rm load}$,

$$Z_{\rm acc} = \frac{1}{2}\left[\exp\left(\frac{\xi_{\rm acc}}{\xi_{\rm load}}\right) + \exp\left(-\frac{\xi_{\rm acc}}{\xi_{\rm load}}\right)\right] = 74\mu_e, \tag{6}$$

and μ_e is the electron mean molecular weight of the ambient medium ($\mu_e = 1$ for hydrogen and $\mu_e = 2$ for helium or heavy

[6] The exit time $\Delta/c\gamma^2$ is much shorter than R/c at $R > R_{\rm gap}$ (§ 2.1). The fact that no caustics develop in the front at $R > R_{\rm gap}$ formally follows from eq. (12) in B02, which shows that density remains finite at all ϖ, while a caustic would correspond to infinite density. At an earlier stage, $R < R_{\rm gap}$, which is not considered in this paper, caustics do develop (see B02).

ions). The numerical value of $\xi_{\rm load} = 20$–30 depends on the precise spectrum of the γ-rays; however, all the other relations remain the same.

The standard GRB spectrum is a broken power law with a peak at $h\nu \approx m_e c^2$,

$$F_\nu = F_1 \begin{cases} \left(\dfrac{h\nu}{m_e c^2}\right)^{-\alpha_1}, & h\nu < m_e c^2, \\ \left(\dfrac{h\nu}{m_e c^2}\right)^{-\alpha_2}, & h\nu > m_e c^2. \end{cases} \quad (7)$$

When observed from a redshift $z \approx 1$, the spectrum peaks at $h\nu \approx 250$ keV, as reported by Burst and Transient Source Experiment (BATSE) observations (Preece et al. 2000). The parameter $\xi_{\rm load}$ for such a spectrum was derived in B02,

$$\xi_{\rm load}(\alpha_1,\ \alpha_2) = \frac{(\alpha_2 - \alpha_1)}{(1-\alpha_1)(\alpha_2 - 1)} \left(\frac{\alpha_2 - \alpha_1}{2\phi \epsilon_{\rm KN}^{\alpha_2 - \alpha_1}}\right)^{1/2}, \quad (8)$$

where $\epsilon_{\rm KN} \approx 0.4$ and $\phi = (7/12)2^{-\alpha_2}(1+\alpha_2)^{-5/3}$. In the examples below we fix $\alpha_1 = 0$, so that

$$\xi_{\rm load}(\alpha_2) = \left(\frac{6}{7}\right)^{1/2} \frac{5^{\alpha_2/2}\alpha_2^{3/2}}{\alpha_2 - 1}(1+\alpha_2)^{5/6}. \quad (9)$$

A typical GRB has $\alpha_2 \approx 1.5$, which gives $\xi_{\rm load} \approx 24$.

At sufficiently large radii, when the γ-ray front has $\xi < \xi_{\rm load}$, its effect on the medium is negligible: the medium remains almost static ($\gamma \approx 1$) and $e^\pm$-free ($Z \approx 1$). When the front has $\xi > \xi_{\rm load}$, the runaway $e^\pm$ loading occurs. The number of loaded pairs depends exponentially on ξ as long as $\xi < \xi_{\rm acc}$. At $\xi > \xi_{\rm acc}$, the front acts as a relativistic accelerator and the dependence of γ and Z on ξ can be approximated by power laws (eqs. [4] and [5]). The slopes of $\gamma(\xi)$ and $Z(\xi)$ change at $\xi \approx 3\xi_{\rm acc}$ where $Z \approx 10^3$ and the mass of injected $e^\pm$ is comparable to that of the ambient ions. An interesting effect takes place at $\xi > \xi_{\rm gap} \approx 3\times10^3$: then $\gamma(\xi)$ exceeds the Lorentz factor of the ejecta $\Gamma_{\rm ej} = 10^2$–10^3. The radiation front with such a high ξ pushes the external medium away from the fireball and opens a gap, so that the fireball moves in a cavity cleared by its own radiation front.

The γ-ray front expands with time, and its ξ-parameter decreases as R^{-2}. It starts at very high ξ and then passes through $\xi_{\rm gap}$, $\xi_{\rm acc}$, and $\xi_{\rm load}$ at radii $R_{\rm gap}$, $R_{\rm acc}$, and $R_{\rm load}$, respectively,

$$R_{\rm acc} \approx 7\times10^{15}\left(\frac{E_\gamma}{10^{53}\ {\rm ergs}}\right)^{1/2}\ {\rm cm},$$
$$R_{\rm load} = (5 + \ln\mu_e)^{1/2} R_{\rm acc}, \quad R_{\rm gap} \approx \frac{R_{\rm acc}}{3}. \quad (10)$$

The $Z(R)$ and $\gamma(R)$ of the preshock medium are shown in Figure 2 for $E_\gamma = 10^{53}$ ergs. They do not depend on the density of the ambient medium as long as the medium is optically thin and are entirely determined by the parameters of the radiation front. The figure shows the exact Z and γ (see also Figs. 1 and 3 in B02) and their analytical approximations (eqs. [4] and [5]).

Variations in GRB spectra have some effect on $Z(R)$ and $\gamma(R)$ because they affect $\xi_{\rm load}$. For instance, if α_2 changes from 1.5 to 2, then $\xi_{\rm load}$ changes from 24 to 33 (eq. [9]); the resulting changes in $Z(R)$ and $\gamma(R)$ are shown in Figure 2.

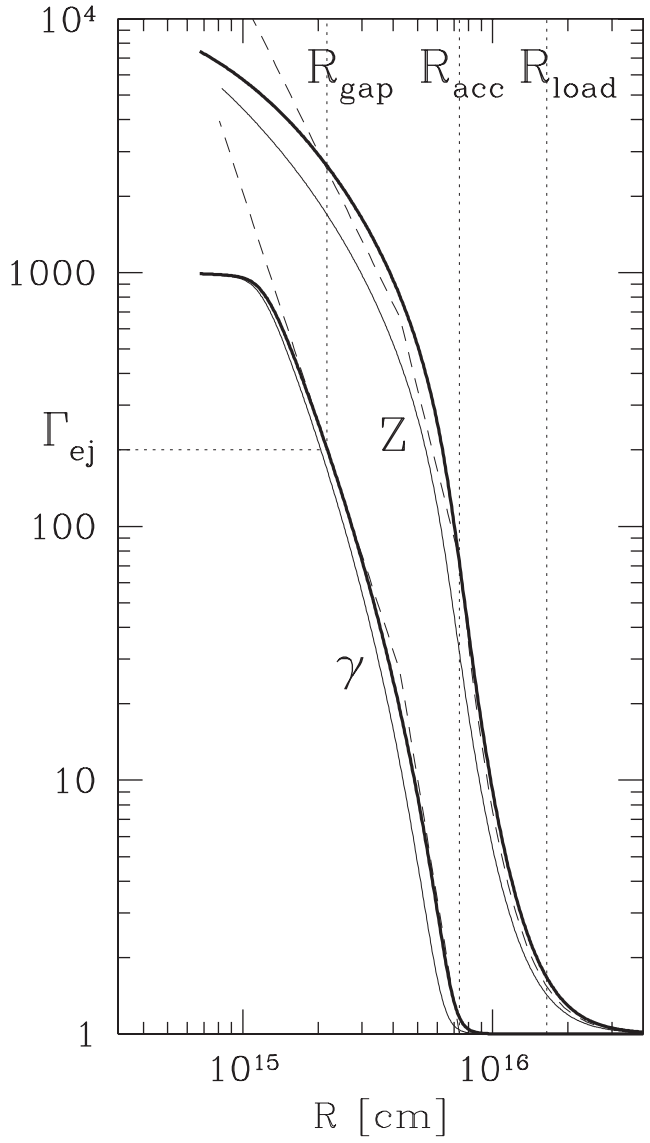

FIG. 2.—Pair-loading factor Z and Lorentz factor γ acquired by a medium at a radius R when it is overtaken by a γ-ray front. The front has isotropic energy $E_\gamma = 10^{53}$ ergs. The exact numerical results are shown by solid lines and the analytical approximation (eqs. [4] and [5]) by dashed lines. The characteristic radii $R_{\rm gap}$, $R_{\rm acc}$, and $R_{\rm load}$ are indicated by vertical dotted lines. The condition $\gamma = \Gamma_{\rm ej}$ defines $R_{\rm gap}$; in this example $\Gamma_{\rm ej} = 200$ (shown by the horizontal dotted line). $Z(R)$ and $\gamma(R)$ for different E_γ are found by simple rescaling $R \rightarrow (E_\gamma/10^{53})^{1/2}R$. The GRB spectrum assumed in the calculation has the typical high-energy slope $\alpha_2 = 1.5$. To illustrate the dependence on α_2, we also show $Z(R)$ and $\gamma(R)$ for $\alpha_2 = 2$ (*thin solid lines*).

2.2. *Blast Wave*

The prompt GRB emission can be produced quite early inside the fireball, preceding the development of the external blast wave at $R \sim 10^{15}$–10^{17} cm. (The millisecond variability observed in GRBs suggests small radii of γ-ray emission, $R_\gamma \sim 10^{12}$–10^{14} cm.) We assume that the γ-rays are emitted before the afterglow and then propagate ahead of the blast wave through the ambient medium.

Then three characteristic radii $R_{\rm gap}$, $R_{\rm acc}$, and $R_{\rm load}$ define four stages of the GRB explosion:

1. $R < R_{\rm gap}$. The fireball moves in a cavity cleared by its radiation front. The $e^\pm$-rich external medium ($Z > 10^3$) surfs ahead with $\gamma > \Gamma_{\rm ej}$.

2. $R_{\rm gap} < R < R_{\rm acc}$. The external blast wave has formed, and the fireball sweeps up the $e^{\pm}$-rich medium ($Z \gtrsim 10^2$) that moves with $1 \ll \gamma < \Gamma_{\rm ej}$.

3. $R_{\rm acc} < R < R_{\rm load}$. The fireball sweeps up the static medium ($\gamma \approx 1$) dominated by $e^{\pm}$ ($Z \gg 1$).

4. $R > R_{\rm load}$. The fireball sweeps up the static pair-free medium.

The blast wave develops at $R > R_{\rm gap}$, with its forward and reverse shocks. The preshock external medium is $e^{\pm}$-rich and moving relativistically, which affects the jump conditions and the state of the postshock plasma. At $R = R_{\rm gap}$ the blast wave gently begins to sweep up the preaccelerated medium with a small relative Lorentz factor $\Gamma_{\rm rel} \approx 1$ ($\Gamma_{\rm ej} \approx \gamma$). With increasing $R > R_{\rm gap}$, γ falls off quickly and approaches unity at $R = R_{\rm acc}$ as $\gamma = (R/R_{\rm acc})^{-6}$. Thus, the fireball suddenly "learns" that there is an interesting amount of slow material in its way and hits it with a large $\Gamma_{\rm rel}$. This resembles a collision with a wall and results in a sharp rise of the afterglow at $R \approx R_{\rm acc}$ (B02).

The explosion picture is modified if the γ-ray front is created by the shock wave itself (external model of the prompt GRB) rather than by internal dissipation in the fireball. Then a self-consistent blast wave model exists without the gap. A sufficiently dense medium can complicate that picture if it leads to an "electromagnetic catastrophe" in the forward shock (Stern 2003), i.e., a runaway production of γ-rays, which may result in transient gap openings.

The uncertainties in the mechanism of the prompt GRB play little role for the afterglow model developed below as we focus on the stage when the process of γ-ray production is over. We consider $R > R_{\rm gap}$, and the blast wave at these radii has practically no memory of the gap opening. We need only to know the parameters of the emitted γ-ray front (eq. [7]), which are taken from observations. Therefore, the following calculations apply to both internal and external models of the prompt GRB emission.

3. AFTERGLOW CALCULATION

The production of afterglows without the $e^{\pm}$-loading effects, i.e., with $Z = 1$ and $\gamma = 1$, was studied previously in detail. The electrons were assumed to receive a significant fraction $\epsilon_e \sim 0.1$ of the shock energy (the remaining fraction $1 - \epsilon_e$ is carried by the postshock ions). This leads to a high energy per electron, and the early high-Γ blast wave emits hard X-rays in the fast-cooling regime: the electrons immediately radiate the received energy, practically at the same radius where they are shocked.

The $e^{\pm}$ loading changes the picture: a lot of leptons now share the energy received from the shock. As a result, the mean energy per postshock $e^{\pm}$ is reduced by orders of magnitude and $e^{\pm}$ emit much softer radiation. Furthermore, the postshock $e^{\pm}$ can be in the slow-cooling regime so that their emission remains significant at $R > R_{\rm load}$ where no new pairs are added to the blast wave.

3.1. *Formulation of the Problem*

We focus on a sufficiently early stage when $\Gamma > \theta^{-1}$, where θ is the opening angle of the explosion; then the expanding jet behaves like a portion of a spherically symmetric explosion and we can neglect the beaming effects. Three further technical assumptions simplify our calculations:

1. The shocked ambient material is assumed to have a common Lorentz factor Γ (relative motions in the postshock material are subsonic and the assumption of common Γ is good within a factor of $1/\sqrt{3}$).

2. The postshock material is assumed to be in pressure equilibrium, i.e., $P =$ constant throughout this material.

3. When calculating the observed luminosity, we neglect the finite thickness of the blast wave (equal to the distance between the contact discontinuity and the forward shock). The blast wave radiation is then characterized by its total instantaneous luminosity L_ν emitted at a current radius. Inclusion of time delays between photons from different subshells of the blast material would change the result by a factor of a few. A precise calculation of this factor would require one to relax assumptions 1 and 2.

These assumptions allow us to derive the instantaneous luminosity L_ν at a given frequency $\nu_{\rm obs}$. We are interested in the soft emission here, from IR to soft X-rays, and especially optical, $\nu_{\rm obs} \approx 0.5 \times 10^{15}$ Hz.

Consider the moment of time when the blast wave reaches a given radius $\tilde{R}$. The total postshock ambient mass at this moment is[7]

$$\tilde{m}(\tilde{R}) = \int_0^{\tilde{R}} 4\pi R^2 \rho_0(R)\, dR. \tag{11}$$

Each subshell δm of this material has its own history. It used to be a shell of ambient medium located at a radius $R < \tilde{R}$, which was loaded with $e^{\pm}$ pairs and preaccelerated by the prompt γ-rays, then immediately shocked and picked up by the relativistic blast wave. The radius where all that happened is related to m by equation

$$m = \int_0^{R(m)} 4\pi R^2 \rho_0(R)\, dR. \tag{12}$$

Then δm cooled radiatively and adiabatically as the blast wave expanded to the present radius $\tilde{R}$.

We need to evaluate the contribution of each δm to the current luminosity $L_\nu(\tilde{R})$ and therefore have to resolve the blast wave material in its (Lagrangian) mass coordinate $0 < m < \tilde{m}$, even though we do not resolve it in radius and assume that all δm are located at the same $\tilde{R}$. Here $m \to 0$ is the material that was swept up first (at small radii), and $m \to \tilde{m}$ is the currently shocked material. L_ν is the sum of current emissions δL_ν from all δm.

In afterglow models without $e^{\pm}$ loading the emission from $m \ll \tilde{m}$ is negligible, and the instantaneous luminosity is dominated by the recently shocked mass shell $m \lesssim \tilde{m}$. A special feature of pair-loaded blast waves is that their L_ν peaks at $m \ll \tilde{m}$. Therefore, an accurate integration over m is needed.

To calculate δL_ν from each δm, we need to know the current $e^{\pm}$ spectrum $\tilde{f}(\gamma_e)$ and magnetic field $\tilde{B}$ in δm.

3.2. *Magnetic Field*

The magnetic field in shell δm in the blast wave of radius $\tilde{R}$ is given in terms of the customary equipartition parameter $\tilde{\epsilon}_B(m) < 1$,

$$\tilde{U}_B(m) = \frac{\tilde{B}^2(m)}{8\pi} = \tilde{\epsilon}_B(m)\tilde{U}, \tag{13}$$

where $\tilde{U} = 3\tilde{P}$ is the current energy density in the blast wave and $\tilde{P}$ is its pressure. The variables $\tilde{P}$ and $\tilde{U}$ are assumed to be

[7] Hereafter quantities taken at the current radius $\tilde{R}$ are marked by a tilde to distinguish them from the corresponding quantities at radius $R(m)$ where shell $(m,\ m + \delta m)$ was shocked.

constant throughout the postshock material in our simplified model. They are functions of $\tilde{R}$ only and related to the ambient density by the jump condition at the shock front,

$$\tilde{U} = 3\tilde{P} = 4\tilde{\rho}_0 c^2 \tilde{\Gamma}_{\rm rel}\tilde{\Gamma}, \tag{14}$$

where

$$\tilde{\Gamma}_{\rm rel} = \frac{\tilde{\Gamma}}{\tilde{\gamma}(1+\tilde{\beta})} \tag{15}$$

(when $\tilde{\gamma} \ll \tilde{\Gamma}$) is the current Lorentz factor of the preshock medium relative to the blast wave, and $\tilde{\gamma} = (1-\tilde{\beta}^2)^{-1/2}$ is the Lorentz factor of the preshock medium in the laboratory frame. The jump condition given by equation (14) takes into account the compression of the ambient medium preaccelerated to a Lorentz factor $\tilde{\gamma}$ (Madau & Thompson 2000; B02). Thus, the magnetic field can be written as

$$\tilde{B} = \tilde{\Gamma}\left[\frac{32\pi\tilde{\epsilon}_B\tilde{\rho}_0 c^2}{\tilde{\gamma}(1+\tilde{\beta})}\right]^{1/2} = 0.39\tilde{\Gamma}\left[\frac{\tilde{\epsilon}_B\tilde{n}_0\mu_e}{\tilde{\gamma}(1+\tilde{\beta})}\right]^{1/2}\ {\rm G}, \tag{16}$$

where $\tilde{n}_0$ is expressed in cm^{-3}.

The parameter $\tilde{\epsilon}_B(m)$ can change with $\tilde{R}$: the magnetic field evolves as δm expands from the radius R where it was shocked to the current radius $\tilde{R}$. The toroidal field component is dominant in the expanding shocked plasma and, if the magnetic flux is conserved, $\tilde{B}$ evolves as

$$\frac{\tilde{B}(m)}{B(m)} = \frac{\tilde{\rho}}{\rho}\frac{\tilde{R}}{R} = \left(\frac{\tilde{P}}{P}\right)^{3/4}\frac{\tilde{R}}{R}, \tag{17}$$

where ρ is the proper mass density of baryons and we have used the adiabatic equation of state $P \propto \rho^{4/3}$. Using equation (14), we can rewrite the flux conservation condition as

$$\frac{\tilde{B}(m)}{B(m)} = \left(\frac{\tilde{\Gamma}\tilde{\Gamma}_{\rm rel}\tilde{\rho}_0}{\Gamma\Gamma_{\rm rel}\rho_0}\right)^{3/4}\frac{\tilde{R}}{R}, \quad \frac{\tilde{\epsilon}_B}{\epsilon_B} = \left(\frac{\tilde{\Gamma}\tilde{\Gamma}_{\rm rel}\tilde{\rho}_0}{\Gamma\Gamma_{\rm rel}\rho_0}\right)^{1/2}\left(\frac{\tilde{R}}{R}\right)^2. \tag{18}$$

It shows that $\tilde{\epsilon}_B$ grows downstream of the shock. This growth, however, cannot proceed beyond equipartition: $\tilde{\epsilon}_B$ then saturates near unity.

If the flux is not conserved (the magnetic field may reconnect/dissipate in the blast), the evolution of postshock $\tilde{B}$ is different. Therefore, we do not specify $\tilde{\epsilon}_B$ in the calculations until the last step when we give examples. Then, besides equation (18) we also consider the case of $\tilde{\epsilon}_B = \epsilon_B = {\rm const}$, which is a second reasonable prescription for the magnetic field evolution.

3.3. *Distribution Function of Electrons/Positrons*

The customary phenomenological shock model of GRBs assumes that the electrons (and positrons) are impulsively accelerated at the shock front with a power-law spectrum,

$$f(\gamma_e) = \begin{cases} 0, & \gamma_e < \gamma_m, \\ K\left(\dfrac{\gamma_e}{\gamma_m}\right)^{-p}, & \gamma_e > \gamma_m. \end{cases} \tag{19}$$

This initial spectrum is injected in δm at the radius $R(m)$ where δm is shocked; the Lorentz factor γ_e of the accelerated leptons is measured in the fluid frame. The total injected energy of nonthermal $e^{\pm}$ in this frame is

$$\delta E = \int \gamma_e m_e c^2 f(\gamma_e)\, d\gamma_e = \epsilon_e \Gamma_{\rm rel}\, \delta m\, c^2, \tag{20}$$

and the total number of nonthermal leptons in δm is

$$\delta N = \int f(\gamma_e)\, d\gamma_e = \left(\frac{\delta m}{\mu_e m_p}\right) Z. \tag{21}$$

Here $p > 2$ and $\epsilon_e < 1$ are phenomenological parameters of the electron acceleration.

From equations (20) and (21) one finds γ_m and K,

$$\gamma_m = \frac{\Gamma_{\rm rel}}{(Z/\mu_e)}\frac{\epsilon_e(p-2)m_p}{(p-1)m_e}, \tag{22}$$

$$K = (p-1)\frac{\delta N}{\gamma_m}. \tag{23}$$

When a shocked δm expands from R to $\tilde{R}$, the injected nonthermal spectrum is modified by two effects:

1. Adiabatic cooling shifts the whole $e^{\pm}$ distribution as $\gamma_e \propto P^{1/4}$, retaining the power-law shape. The minimum Lorentz factor of the nonthermal spectrum, γ_m, changes by the factor

$$A = \left(\frac{\tilde{P}}{P}\right)^{1/4} = \left(\frac{\tilde{\rho}_0\tilde{\Gamma}_{\rm rel}\tilde{\Gamma}}{\rho_0\Gamma_{\rm rel}\Gamma}\right)^{1/4}, \tag{24}$$

$$\tilde{\gamma}_m(m,\ \tilde{R}) = A\gamma_m(m,\ R), \tag{25}$$

and the normalization K of the spectrum changes as $\tilde{K} = K/A$.

2. Radiative cooling cuts off the $e^{\pm}$ distribution at high γ_e. In most of the models considered below, the exact position of the cutoff is not important because we focus on the low-frequency radiation. The cutoff can be estimated as follows.

The radiative cooling of δm can peak at any radius R' between R and $\tilde{R}$, and then the cutoff is shaped at this radius. Electrons with Lorentz factor γ_e are cooled with a rate (assuming isotropic pitch-angle distribution)

$$\dot{\gamma}_e = -\frac{4}{3}\frac{\sigma_{\rm T}}{m_e c}\left(\frac{B'^2}{8\pi} + U'_s\right)\gamma_e^2, \tag{26}$$

where $B' = B(m,\ R')$ and $U'_s = U_s(m,\ R')$ is the energy density of soft (synchrotron) radiation in δm at radius R'. We assume that the bulk of synchrotron radiation in the fluid frame satisfies $h\nu_{\rm fluid} < m_e c^2/\gamma_e$ and scatters off $e^{\pm}$ with Thomson cross section. Using equations (13) and (14), we get

$$\dot{\gamma}_e = -\frac{16}{3}\frac{\rho'_0}{m_e}\sigma_{\rm T} c \epsilon'_B \Gamma'_{\rm rel}\Gamma'(1+C')\gamma_e^2. \tag{27}$$

Here $C' = U'_s/U'_B$ is the relative contribution of inverse Compton scattering to the cooling rate.

The characteristic cooling Lorentz factor γ'_c at R' is defined by the condition that the cooling timescale $\gamma_e/|\dot{\gamma}_e|$ equals the expansion timescale $(R'-R)/\Gamma' c$. This yields

$$\gamma'_c(m) = \frac{3m_e}{16\epsilon'_B\Gamma'_{\rm rel}\sigma_{\rm T}(1+C')(R'-R)\rho'_0}. \tag{28}$$

Note that C' depends on the radiated energy U'_s, which in turn depends on γ'_c; therefore, equation (28) is implicit. It can be solved as follows. The total radiation density in δm is comparable to the lost $e^{\pm}$ energy: $U'_{\rm rad} \approx (\gamma'_c/\gamma'_m)^{2-p}\epsilon_e U'$ if $\gamma'_c > \gamma'_m$ and $U'_{\rm rad} \approx \epsilon_e U'$ otherwise. Its synchrotron fraction is $U'_s/U'_{\rm rad} = U'_B/(U'_s + U'_B)$. This allows one to express $C' = U'_s/U'_B$ in terms of γ'_c,

$$C'(C'+1) = \frac{\epsilon_e}{\epsilon'_B}\begin{cases} 1, & \gamma'_c < \gamma'_m, \\ \left(\dfrac{\gamma'_c}{\gamma'_m}\right)^{2-p}, & \gamma'_c > \gamma'_m. \end{cases} \tag{29}$$

Now we have two equations (28) and (29), which can be solved for C' and γ'_c.

This estimate assumes that $U'_s(m)$ is produced locally at a given m and neglects the transport of synchrotron radiation across the blast wave. Inclusion of transport further complicates the calculation of $C'(m)$ and $\gamma'_c(m)$. In this paper we avoid models with significant Compton cooling and use the simple estimate of γ'_c (eq. [28]) with $C' = 0$. The consistency of this estimate requires $C'(\gamma'_c) \lesssim 1$, which can be checked using equation (29). An estimate of Compton cooling that includes the radiation transport will be given in § 6.3.

The $e^{\pm}$ distribution cutoff $\tilde{\gamma}_c$ in δm at the current radius $\tilde{R}$ is

$$\tilde{\gamma}_c = \gamma'_c A', \quad A' = \left(\frac{\tilde{\rho}_0 \tilde{\Gamma}_{\rm rel}\tilde{\Gamma}}{\rho'_0 \Gamma'_{\rm rel}\Gamma'}\right)^{1/4}. \tag{30}$$

It is shaped at the radius R' where $(\gamma'_c A')$ is minimum with γ'_c calculated as described above, and its evolution from R' to $\tilde{R}$ is determined by the adiabatic cooling factor A'.

If $\tilde{\gamma}_m < \tilde{\gamma}_c$ (slow-cooling regime), the current nonthermal $e^{\pm}$ distribution in δm is a power law with slope p and normalization $\tilde{K}$, extending from $\tilde{\gamma}_m$ to $\tilde{\gamma}_c$. If $\tilde{\gamma}_c < \tilde{\gamma}_m$ (fast-cooling regime), all nonthermal leptons δN pile up near a single Lorentz factor $\gamma_e \approx \tilde{\gamma}_c$. In any case, the number of nonthermal $e^{\pm}$ in δm is given by equation (21), so their distribution function at $\tilde{R}$ can be written as

$$\tilde{f}(\gamma_e) = \delta N\begin{cases} \dfrac{(p-1)}{\tilde{\gamma}_m}\left(\dfrac{\gamma_e}{\tilde{\gamma}_m}\right)^{-p} H(\gamma_e - \tilde{\gamma}_m)H(\tilde{\gamma}_c - \gamma_e), & \tilde{\gamma}_m < \tilde{\gamma}_c, \\ \delta(\gamma_e - \tilde{\gamma}_c), & \tilde{\gamma}_m > \tilde{\gamma}_c, \end{cases} \tag{31}$$

where $H(\ldots)$ is the Heaviside step function and $\delta(\ldots)$ is the Dirac δ-function.

3.4. *Self-Absorption*

Self-absorption can affect synchrotron emission from $e^{\pm}$ with low γ_e. The low-γ_e population is created at the very beginning of pair loading ($R < R_{\rm acc}$) when the preacceleration γ is significant, the forward shock is relatively mild ($\Gamma_{\rm rel} \ll \Gamma$), and the pair-loading factor Z is comparable to 10^3 (see eq. [22]). The low-energy postshock $e^{\pm}$ are slowly cooling and produce low-frequency radiation that is self-absorbed.

Self-absorption is, however, not important for blast wave radiation with frequencies $\nu \gtrsim 10^{12}$ Hz that we consider thereafter. This radiation is dominated by the blast wave material with sufficiently high γ_m so that self-absorption can be neglected for all $\gamma_e \geq \gamma_m$. The condition of small self-absorption can be written as $U_m < \gamma_m m_e c^2 (\nu/c)^3$, where U_m is the density of synchrotron radiation produced by $e^{\pm}$ with $\gamma_e = \gamma_m$, and we assume thereafter

$$U_m \sim \gamma_m^2 U_B \sigma_{\rm T}\frac{R}{\Gamma} < \gamma_m m_e c^2 \left(\frac{\nu}{c}\right)^3. \tag{32}$$

This roughly corresponds to $\nu > 10^{12}$ Hz.

3.5. *Synchrotron Luminosity*

Given the current magnetic field $\tilde{B}$ and nonthermal $e^{\pm}$ spectrum $\tilde{f}(\gamma_e)$ in δm, it is straightforward to evaluate its contribution δL_ν to the instantaneous luminosity of the blast wave.

The synchrotron spectrum of $e^{\pm}$ with Lorentz factors γ_e in the fluid frame peaks at the frequency (assuming isotropic pitch-angle distribution)

$$\nu_{\rm fluid} \approx 0.15\frac{e\tilde{B}}{m_e c}\gamma_e^2. \tag{33}$$

The intensity-weighted Doppler shift to the laboratory frame is given by

$$\nu = \frac{4}{3}\tilde{\Gamma}\nu_{\rm fluid}, \tag{34}$$

and the corresponding observed frequency is

$$\nu_{\rm obs} = \frac{\nu}{1+z}, \tag{35}$$

where z is the cosmological redshift of the burst. From equation (33) we find γ_e of $e^{\pm}$ whose synchrotron spectrum peaks at a given ν. We denote this characteristic Lorentz factor by $\tilde{\gamma}_\nu$,

$$\tilde{\gamma}_\nu \equiv \gamma_\nu(m,\ \tilde{R}) \approx \left(\frac{5\nu m_e c}{\tilde{\Gamma} e\tilde{B}}\right)^{1/2}. \tag{36}$$

The emitted synchrotron power by the $\tilde{\gamma}_\nu$ electron is $\dot{E}_s = \sigma_{\rm T} c\tilde{B}^2\tilde{\gamma}_\nu^2/6\pi$, and the synchrotron luminosity from an $e^{\pm}$ population with distribution $dN/d\gamma_e$ is approximately given by

$$\nu L_\nu = \frac{dL}{d\log\nu} = \frac{dL}{2d\log\tilde{\gamma}_\nu} = \frac{1}{2}\left(\gamma_e\frac{dN}{d\gamma_e}\right)_{\gamma_e=\tilde{\gamma}_\nu}\dot{E}_s(\gamma_\nu). \tag{37}$$

The $e^{\pm}$ population in δm peaks near $\tilde{\gamma}_m$ if $\tilde{\gamma}_c > \tilde{\gamma}_m$ (slow-cooling regime) and near $\tilde{\gamma}_c$ if $\tilde{\gamma}_c < \tilde{\gamma}_m$ (fast-cooling regime). In the first case, the synchrotron luminosity of δm can be written as

$$\delta(\nu L_\nu) = \delta(\nu_{\rm fluid}L_{\nu_{\rm fluid}}) = \delta L^{\max}\begin{cases} \left(\dfrac{\tilde{\gamma}_\nu}{\tilde{\gamma}_m}\right)^{2/3}, & \tilde{\gamma}_\nu < \tilde{\gamma}_m < \tilde{\gamma}_c, \\ \left(\dfrac{\tilde{\gamma}_\nu}{\tilde{\gamma}_m}\right)^{1-p}, & \tilde{\gamma}_m < \tilde{\gamma}_\nu < \tilde{\gamma}_c, \\ 0, & \tilde{\gamma}_m < \tilde{\gamma}_c < \tilde{\gamma}_\nu, \end{cases} \tag{38}$$

where

$$\delta L^{\max} \approx \frac{\sigma_{\rm T} c\tilde{B}^2}{12\pi}\tilde{\gamma}_\nu^2\,\delta N = \frac{5}{12\pi}\frac{m_e c^2\sigma_{\rm T}}{e}\frac{\tilde{B}}{\tilde{\Gamma}}\nu\,\delta N. \tag{39}$$

Note that $\delta(\nu L_\nu)$ is originally defined as energy emitted per unit time in the fixed laboratory frame; however, we calculate it in the fluid frame using the Lorentz invariancy of νL_ν. The

parameter $\delta L^{\max}$ is a maximum luminosity that would be emitted at ν at the most favorable condition $\tilde{\gamma}_m = \tilde{\gamma}_\nu$. [In this case $2\delta(\nu L_\nu)$ equals the energy-loss rate of the dominant $e^\pm$ population with $\gamma_e \sim \gamma_m$.] Similarly, in the fast-cooling regime, we have

$$\delta(\nu L_\nu) = \delta L^{\max} \begin{cases} \left(\dfrac{\tilde{\gamma}_\nu}{\tilde{\gamma}_c}\right)^{2/3}, & \tilde{\gamma}_\nu < \tilde{\gamma}_c < \tilde{\gamma}_m, \\ 0, & \tilde{\gamma}_\nu > \tilde{\gamma}_c. \end{cases} \quad (40)$$

The nonthermal $e^\pm$ with Lorentz factors $\gamma_e = \tilde{\gamma}_m$ and $\gamma_e = \tilde{\gamma}_c$ emit radiation at frequencies

$$\tilde{\nu}_m = 0.2\tilde{\Gamma}\frac{e\tilde{B}}{m_e c}\tilde{\gamma}_m^2, \quad \tilde{\nu}_c = 0.2\tilde{\Gamma}\frac{e\tilde{B}}{m_e c}\tilde{\gamma}_c^2, \quad (41)$$

and the spectral luminosity $\delta L_\nu/\delta m$ at a Lagrangian coordinate m can be written as

$$\frac{\delta L_\nu}{\delta m} = \frac{\delta L_\nu^{\max}}{\delta m} \begin{cases} \left(\dfrac{\nu}{\tilde{\nu}_m}\right)^{1/3}, & \nu < \tilde{\nu}_m < \tilde{\nu}_c, \\ \left(\dfrac{\nu}{\tilde{\nu}_m}\right)^{(1-p)/2}, & \tilde{\nu}_m < \nu < \tilde{\nu}_c, \\ \left(\dfrac{\nu}{\tilde{\nu}_c}\right)^{1/3}, & \nu < \tilde{\nu}_c < \tilde{\nu}_m, \\ 0, & \nu > \tilde{\nu}_c. \end{cases} \quad (42)$$

An explicit formula for $\delta L_\nu^{\max} = \delta L^{\max}/\nu$ is found using equation (21) for δN and equation (16) for $\tilde{B}$,

$$\frac{\delta L_\nu^{\max}}{\delta m} = \frac{5}{12\pi}\frac{m_e c^2 \sigma_{\rm T}}{e}\frac{\tilde{B}}{\tilde{\Gamma}}\frac{\delta N}{\delta m} \approx c^2\left[32\pi\frac{m_e}{\mu_e m_p}\frac{\tilde{\epsilon}_B \tilde{n}_0 r_e^3}{\tilde{\gamma}(1+\tilde{\beta})}\right]^{1/2} Z$$
$$\approx 30\left[\frac{\tilde{\epsilon}_B \tilde{n}_0}{\mu_e \tilde{\gamma}(1+\tilde{\beta})}\right]^{1/2} Z, \quad (43)$$

where $r_e = e^2/m_e c^2 \approx 2.81\times10^{-13}$ cm is the classical electron radius. Note that $\delta L_\nu^{\max}/\delta m$ does not depend on ν.

The total instantaneous luminosity of the blast wave is found by integrating over m,

$$L_\nu(\tilde{R}) = \int_0^{\tilde{m}} \frac{\delta L_\nu}{\delta m}\, \delta m. \quad (44)$$

3.6. *Observed Flux*

An observer at a distance D much smaller than the Hubble scale would measure the spectral luminosity (e.g. Rybicki & Lightman 1979),

$$L_\nu^{\rm obs}(\tilde{R}) = \frac{4}{3}\tilde{\Gamma}^2 L_\nu, \quad (45)$$

and the spectral flux $F_\nu = L_\nu^{\rm obs}/4\pi D^2$. For cosmologically large D, the flux formula is modified by two effects: D is replaced by the luminosity distance and the observed frequency of radiation is redshifted, $\nu_{\rm obs} = (1+z)^{-1}\nu$,

$$F_\nu = \frac{\nu L_\nu^{\rm obs}}{4\pi\nu_{\rm obs} D^2} = \frac{\tilde{\Gamma}^2(1+z)}{3\pi D^2} L_\nu, \quad (46)$$

where

$$D = \frac{2c}{H_0}\left(1+z-\sqrt{1+z}\right) \approx 2.6\times10^{28}\left(1+z-\sqrt{1+z}\right)\ {\rm cm}, \quad (47)$$

and $H_0 \approx 70$ km s^{-1} Mpc^{-1} is the Hubble constant. The formula for D assumes a simple model of matter-dominated flat universe and may be easily modified to include the cosmological constant. The observed optical magnitude in V or R band is related to F_ν by

$$m_V = 8.873 - 2.5\log F_\nu, \quad m_R = 8.645 - 2.5\log F_\nu, \quad (48)$$

where F_ν is in units of Jy $= 10^{-23}$ ergs cm^{-2}.

The flux $F_\nu(\tilde{R})$ is received at the observer time

$$t_{\rm obs}(\tilde{R}) \approx \frac{\tilde{R}}{2\tilde{\Gamma}^2 c}(1+z) \quad (49)$$

after the arrival of first photons (prompt γ-rays) from the explosion. More exactly, it is received during a time interval $\Delta t_{\rm obs} \sim (\tilde{R}/2\tilde{\Gamma}^2 c)(1+z)$ because of the spherical curvature and finite thickness of the blast wave, and equation (49) gives only an approximate arrival time. The numerical factor in this equation can vary around $\frac{1}{2}$ by a factor of $\sim$2, depending on the blast wave dynamics $\tilde{\Gamma}(\tilde{R})$. We hereafter use the approximate equation (49) with the fixed factor $\frac{1}{2}$. This degree of accuracy is consistent with our approximate treatment of the blast wave as a constant-pressure shell.

4. NUMERICAL EXAMPLES

It is straightforward to calculate the afterglow emission $F_\nu(t_{\rm obs})$ using the formulae of § 3 and taking the integral given by equation (44) numerically. A simple illustrative afterglow model has the following parameters:

1. Isotropic energy $E_{\rm ej} = 10^{53}$ ergs and initial Lorentz factor $\Gamma_0 = 200$ (the reverse shock is assumed to be nonrelativistic and $\Gamma_0 \approx \Gamma_{\rm ej}$).
2. External density $n_0(R) =$ const and $\mu_e = 1$ (uniform hydrogen medium). We consider $n_0 = 0.1, 1, 10, 10^2$, and 10^3 cm^{-3}.
3. Parameters of the postshock leptons: $\epsilon_e = 0.1$ and $p = 2.5$. Most of the blast wave energy is carried by relativistically hot ions that do not exchange energy with the electrons and the blast wave is approximately adiabatic.
4. Magnetic equipartition parameter ϵ_B immediately behind the shock. It is taken equal to 10^{-6}, 10^{-4}, or 10^{-2} in the example models. The parameter $\epsilon_B(m,\ \tilde{R})$ can evolve in the postshock material of the blast wave as it expands and decelerates. We consider two cases: magnetic flux is conserved in the postshock region (eq. [18]) or $\epsilon_B(m,\ \tilde{R}) = \epsilon_B$ is constant in all shells m at all times.
5. The γ-ray front is described by its isotropic energy E_γ. In the examples below we assume $E_\gamma = E_{\rm ej} = 10^{53}$ ergs, i.e., half of the total explosion energy is initially emitted in the prompt GRB. We also assume the standard GRB spectrum with a high-energy slope $\alpha_2 = 1.5$, which gives $\xi_{\rm acc} = 120$ (§ 2).

The blast wave has a constant $\Gamma \approx \Gamma_0$ until it approaches the characteristic deceleration radius $R_{\rm dec}$ where the swept-up mass m satisfies $\Gamma_0^2 mc^2 = E_{\rm ej}$. At larger radii $\Gamma(R)$ quickly approaches the self-similar solution of Blandford & McKee (1976): $\Gamma = (17/12)^{1/2}\Gamma_0(R/R_{\rm dec})^{-3/2}$. We use a simple approximation: $\Gamma(R) = \Gamma_0$ at $R \le R_{\rm dec}$ and $\Gamma(R) = \Gamma_0(R/R_{\rm dec})^{-3/2}$ at $R \ge R_{\rm dec}$.

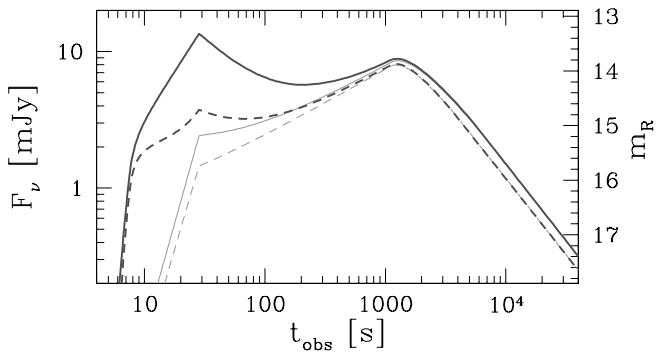

FIG. 3.—Example of the optical light curve in the R band, $\nu_{obs} = 5.45 \times 10^{14}$ Hz, for a "canonical" GRB explosion: adiabatic blast wave with $E_{ej} = E_\gamma = 10^{53}$ ergs, $\Gamma_0 = 200$, $z = 1$, $n_0 = 10$ cm^3, $\epsilon_B = 10^{-4}$, $\epsilon_e = 0.1$, $p = 2.5$. Left axis indicates the observed flux in mJy, and right axis the corresponding R magnitude. Calculations shown by solid lines assume conservation of the postshock magnetic flux. Dashed lines show the results with $\epsilon_B(m, R) = \text{const} = \epsilon_B$ assumption. Thin light curves would be obtained if the pairs were neglected ($Z = 1$ and $\gamma = 1$). [*See the electronic edition of the Journal for a color version of this figure.*]

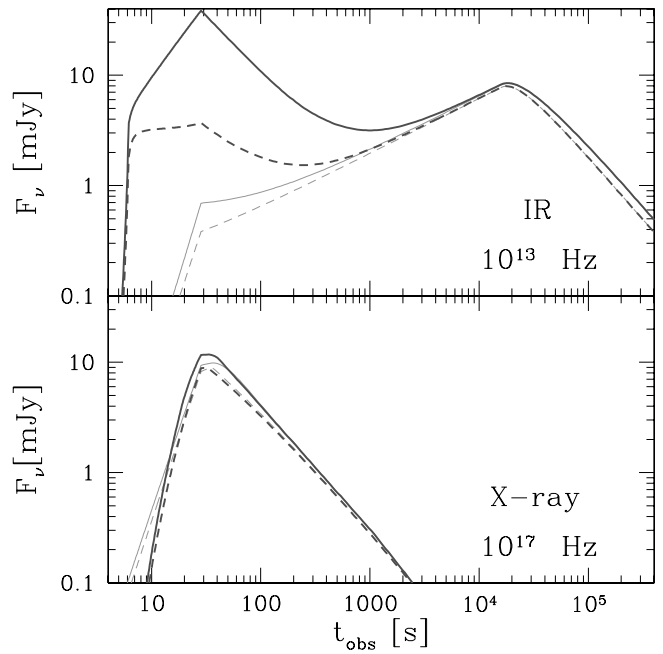

FIG. 4.—Light curves at $\nu_{obs} = 10^{13}$ (*top*) and 10^{17} Hz (*bottom*) for the same model as in Fig. 3. The meaning of line types is the same as in Fig. 3. [*See the electronic edition of the Journal for a color version of this figure.*]

It has sufficient accuracy, adequate to our simplified hydrodynamical model (§ 3).

The results of numerical calculations are shown in Figures 3–7. In all examples, a cosmological redshift $z = 1$ is assumed.

Figure 3 shows the optical light curve $F_\nu(t_{obs})$ found at $n_0 = 10$ cm^{-3} and $\epsilon_B = 10^{-4}$. It has two peaks. The first peak is a result of $e^\pm$ loading (for comparison we show the results with $Z = 1$ and $\gamma = 1$, i.e., with neglected impact of the γ-ray front on the external medium). The figure compares the results obtained with magnetic flux conservation and $\epsilon_B(m, \tilde{R}) = \text{const}$. The $e^\pm$ emission is stronger if the magnetic flux is conserved because it implies a higher $\tilde{\epsilon}_B$; then the peak of $e^\pm$ radiation is reached at $\tilde{R} = R_{dec}$ (see § 5).

The second peak is produced by the pair-free part of the blast. It is well described by the standard afterglow model and corresponds to $\nu_m = \nu$ (see § 5.1). The time of the second peak $t_{peak} \propto (\epsilon_B n_0)^{1/3} \epsilon_e^{4/3} \nu_{15}^{-2/3}$.

Figure 4 shows the corresponding light curves in the infrared and X-ray bands. The relative contribution of $e^\pm$ to the afterglow is higher at lower frequencies, and their effect is negligible in the hard X-ray band. Comparing the light curves in IR, optical, and soft X-rays, one can see that the spectral flux of the $e^\pm$ peak is comparable in all three cases, indicating a small spectral index of $e^\pm$ radiation.

Figure 5 shows the instantaneous broadband spectrum emitted by the blast wave at the deceleration radius R_{dec} (which is 4.6 larger than R_{acc} in the example model). The small $e^\pm$-dominated fraction of the swept-up mass dominates the emission in soft bands. Its spectral slope is small: $|\alpha| \lesssim 0.2$. At high frequencies, $\nu_{obs} > 10^{17}$ Hz, the spectrum is dominated by the pair-free material behind the current position of the shock and well described by the usual pair-free model. In particular, the standard breaks at $\nu_m \sim 10^{18}$ Hz ($\nu^{1/3} \rightarrow \nu^{-(p-1)/2}$) and $\nu_c \sim 10^{20}$ Hz ($\nu^{-(p-1)/2} \rightarrow \nu^{-p/2}$) are seen. (In the top panel, the second [cooling] break occurs at a smaller frequency $\sim 10^{19}$ Hz and is smooth because ν_c happens to be close to ν_m.) The spectrum of the $e^\pm$ emission component has a break at $\nu \sim \nu_m(m_{load}, \tilde{R})$, which is 10^{17} Hz, and cuts off at $\nu > \nu_c(m_{load}, \tilde{R})$. The cutoff frequency is smaller in the top panel because the flux conservation gives a stronger magnetic field (see also Fig. 8 below).

Figure 6 shows the optical light curves for different n_0 and fixed $\epsilon_B = 10^{-4}$. It also illustrates the effect of magnetic flux conservation by comparing it with the results obtained at $\epsilon_B(m, \tilde{R}) = \text{const}$. The $e^\pm$ emission component quickly increases with increasing n_0. It scales as $n_0^{3/2}$ as we show in § 5, and this scaling is observed in Figure 6 for constant-ϵ_B models.

Figure 7 shows how the optical light curve depends on the shock parameter ϵ_B. At $\epsilon_B = 10^{-2}$ the $e^\pm$ are in the fast-cooling regime ($\nu_c < \nu_m$), and most of the pair energy is emitted at earlier times. This produces a bump in the light curve before or

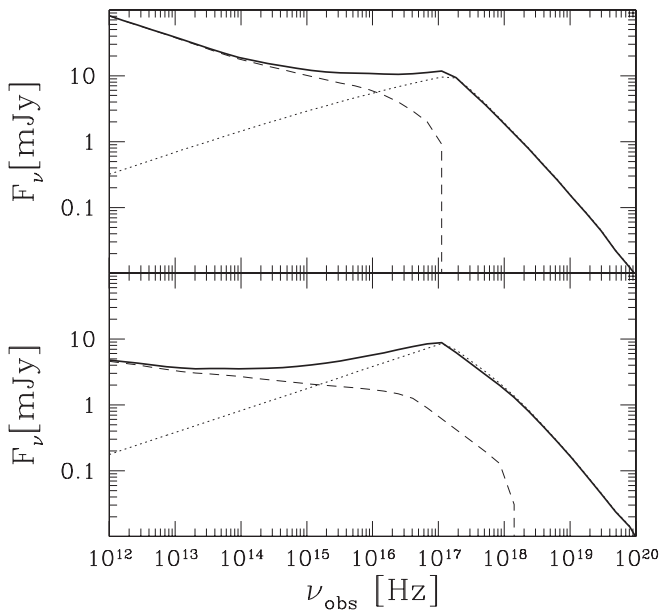

FIG. 5.—Instantaneous spectrum emitted by the blast wave at $R = R_{dec}$ (*solid line*; the model parameters are the same as in Fig. 3). The dashed line shows the contribution of the $e^\pm$-loaded shell $m < m_{load}$. The dotted line shows the spectrum that would be found in the absence of γ-ray front ($Z = 1$ and $\gamma = 1$); it is approximately equal to the spectrum of pair-free material $m > m_{load}$. *Top*: Conservation of postshock magnetic flux is assumed. *Bottom*: $\epsilon_B(m, \tilde{R}) = \text{const} = \epsilon_B$ is assumed.

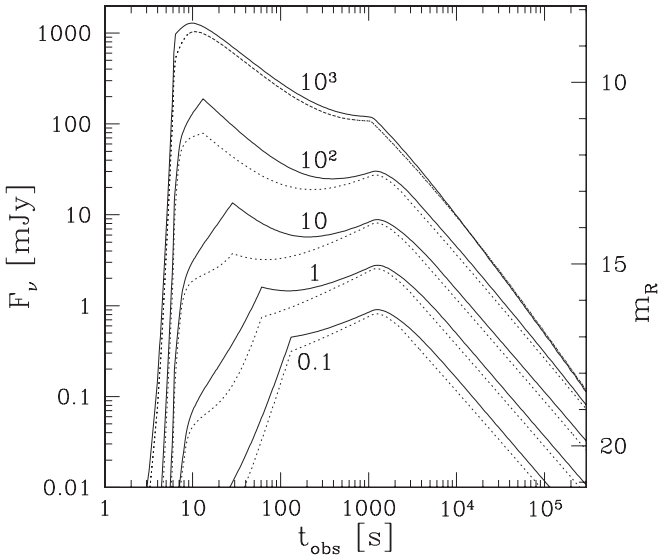

FIG. 6.—Optical light curves found for external densities $n_0 = 0.1$, 1, 10, 10^2, and 10^3 cm^{-3}. All other parameters are the same as in Fig. 3. Calculations shown by solid lines assume conservation of the postshock magnetic flux. Dotted lines show the results with $\epsilon_B(m,\ R) = \text{const} = \epsilon_B$.

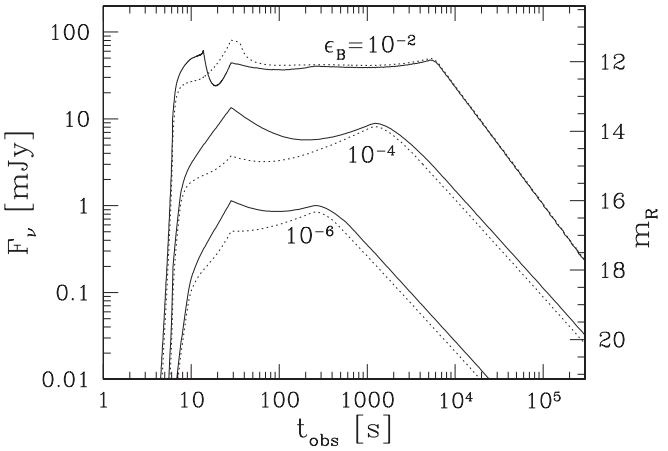

FIG. 7.—Optical light curves found for $\epsilon_B = 10^{-6}$, 10^{-4}, and 10^{-2}. All other parameters are the same as in Fig. 3. Calculations shown by solid lines assume conservation of the postshock magnetic flux. Dotted lines show the results with $\epsilon_B(m,\ R) = \text{const} = \epsilon_B$.

at the deceleration radius, depending on the behavior of magnetic field downstream of the shock.

5. ANALYTICAL CALCULATION

In § 5.1 we derive the luminosity of a relativistic blast wave without a γ-ray precursor, when the $e^{\pm}$-loading and preacceleration effects are neglected ($Z = 1$ and $\gamma = 1$). The pair-free blast wave was studied in a number of previous works (e.g., Sari et al. 1998; Granot et al. 1999; Panaitescu & Kumar 2000) and used extensively to fit observed afterglows. We show that the previous results can be obtained with a different technique where the produced luminosity is calculated as an integral over the Lagrangian mass coordinate m (eq. [44]). This approach is extended to $e^{\pm}$-loaded blast waves in § 5.2.

Where the ambient density profile needs to be specified, we assume a power law, so that the swept-up mass is

$$m(R) = m_{\rm acc}\left(\frac{R}{R_{\rm acc}}\right)^k. \tag{50}$$

The value $k = 3$ describes a uniform medium $n_0(R) = \text{const}$ and $k = 1$ describes a wind-type medium $n_0 \propto R^{-2}$. The derivation in §§ 5.1 and 5.2 applies to both cases. In § 6 we consider in more detail the case $k = 3$.

5.1. *Pair-free Afterglow*

From § 3.4 we have at $Z = 1$ and $\gamma = 1$

$$L^0_\nu = \int_0^{\tilde m} 30\left(\frac{\tilde\epsilon_B \tilde n_0}{\mu_e}\right)^{1/2} \left\{ \begin{array}{ll} \left(\dfrac{\nu}{\tilde\nu_m}\right)^{1/3} & \nu < \tilde\nu_m < \tilde\nu_c \\ \left(\dfrac{\nu}{\tilde\nu_m}\right)^{(1-p)/2} & \tilde\nu_m < \nu < \tilde\nu_c \\ \left(\dfrac{\nu}{\tilde\nu_c}\right)^{1/3} & \nu < \tilde\nu_c < \tilde\nu_m \\ 0 & \nu > \tilde\nu_c \end{array} \right\} dm. \tag{51}$$

The superscript zero in L^0_ν marks the neglect of $e^{\pm}$ loading. Three quantities in the integrand depend on the Lagrangian coordinate m: $\tilde\epsilon_B$, $\tilde\gamma_m$, and $\tilde\gamma_c$. The quantities $\tilde\epsilon_B(m)$ and $\tilde\nu_m(m)$ can vary significantly in the region $m \ll \tilde m$; however, this region makes a negligible contribution to the integral. Therefore, one can approximate $\tilde\epsilon_B$ and $\tilde\nu_m$ as constants: $\tilde\epsilon_B(m) \approx \tilde\epsilon_B(\tilde m)$ and $\tilde\nu_m(m) \approx \tilde\nu_m(\tilde m)$. Only $\tilde\nu_c(m)$ cannot be assumed constant: $\tilde\nu_c(m) \to \infty$ at $m \to \tilde m$.

A characteristic $\tilde\nu_c$ can be defined at $m = \tilde m/2$: it will represent the cooling cutoff in the main part of the postshock material. The value of $\tilde\gamma_c(\tilde m/2)$ is shaped as the blast wave expands from $R = 2^{-1/k}\tilde R$ (the shock radius of $\tilde m/2$) to the current radius $\tilde R$. It is given by (see § 3.3)

$$\tilde\gamma_c\left(\frac{\tilde m}{2}\right) = \frac{am_e}{\sigma_{\rm T} m_p \mu_e n_0 \epsilon_B \tilde\Gamma \tilde R}, \tag{52}$$

where $a \approx (3/16)(1 - 2^{-1/k})^{-1}$ is a numerical factor. We assume here a small Compton factor $C < 1$ for simplicity.

Let us define $\gamma_\nu \equiv \tilde\gamma_\nu(\tilde m/2) \approx \tilde\gamma_\nu(\tilde m)$, $\gamma_m \equiv \tilde\gamma_m(\tilde m/2) \approx \tilde\gamma_m(\tilde m)$, and $\gamma_c \equiv \tilde\gamma_c(\tilde m/2)$; they are given by equations (36), (25), and (52), respectively. The numerical values of these Lorentz factors and the corresponding synchrotron frequencies are[8]

$$\gamma_\nu = 2.7\times10^2 \nu_{15}^{1/2}\Gamma_2^{-1}(\epsilon_B n_0 \mu_e)^{-1/4}, \tag{53}$$

$$\gamma_c = 8.2\times10^2 a R_{16}^{-1}\Gamma_2^{-1}(\epsilon_B n_0 \mu_e)^{-1},$$

$$\nu_c = 9.2\times10^{15} a^2(\epsilon_B n_0 \mu_e)^{-3/2} R_{16}^{-2}\ \text{Hz}, \tag{54}$$

$$\gamma_m = 1.84\times10^5 \Gamma_2 \psi \mu_e,$$

$$\nu_m = 4.6\times10^{20}\Gamma_2^4(\epsilon_B n_0)^{1/2}\psi^2\mu_e^{5/2}\ \text{Hz}, \tag{55}$$

where

$$\psi \equiv \frac{\epsilon_e(p-2)}{(p-1)}. \tag{56}$$

[8] Hereafter in § 5.1 we drop the tilde for $\tilde R$, $\tilde\epsilon_B$, and $\tilde\Gamma$ because there is no need to consider $m \ll \tilde m$ for the pair-free afterglow and distinguish between the postshock and current quantities.

There are two possible cases:

1. $\nu_c > \nu$. Most of the blast material contributes to the observed luminosity at the frequency ν. The luminosity integral over m is then estimated as $\nu L_\nu \approx \tilde{m}(\delta L/\delta m)$, where $\delta L/\delta m$ is taken at $m = \tilde{m}/2$ and given by equation (51) with $\tilde{\nu}_c$ and $\tilde{\nu}_m$ replaced by ν_c and ν_m.
2. $\nu_c < \nu$. Most of the blast material does not emit any synchrotron radiation at ν because its spectrum is cut off at a lower frequency ν_c. Only a mass fraction $(\tilde{m} - m_c) \ll \tilde{m}$ just behind the shock front contributes to L_ν, where m_c is defined by $\tilde{\nu}_c(m_c) = \nu$. The condition $\tilde{\nu}_c > \nu$ is satisfied in the mass interval $m_c < m < \tilde{m}$ and the luminosity integral over m can be estimated as $\nu L_\nu \approx (\tilde{m} - m_c)(\delta L/\delta m)$.

The cooling Lorentz factor $\tilde{\gamma}_c(m)$ increases toward the shock front $\tilde{m}$ as $\tilde{\gamma}_c(m) \propto (\tilde{R} - R)^{-1} \propto (\tilde{m}^{1/k} - m^{1/k})^{-1}$, and we have

$$\frac{\tilde{\gamma}_c(\tilde{m}/2)}{\tilde{\gamma}_c(m)} = \frac{1 - (m/\tilde{m})^{1/k}}{1 - (1/2)^{1/k}} = b\Big(1 - \frac{m}{\tilde{m}}\Big), \tag{57}$$

where so-defined $b(m)$ is a slowly varying function: $b = 2$ at $m = \tilde{m}/2$ and $b = [k(1 - 0.5^{1/k})]^{-1}$ at $m \to \tilde{m}$. Equating $\tilde{\gamma}_c(m)$ and γ_ν, we find m_c,

$$\frac{\tilde{m} - m_c}{\tilde{m}} = \frac{\gamma_c}{b\gamma_\nu} = \frac{1}{b}\left(\frac{\nu_c}{\nu}\right)^{1/2}, \tag{58}$$

with $b = 2$ at $\nu_c = \nu$ and $b = [k(1 - 0.5^{1/k})]^{-1}$ at $\nu_c \ll \nu$. One can take $b \approx 2$ in all cases.

The results can be summarized as follows:

$$L_\nu^0 \approx 30\left(\frac{\epsilon_B n_0}{\mu_e}\right)^{1/2} \tilde{m} g_\nu, \tag{59}$$

$$g_\nu = \frac{1}{1 + b(\nu/\nu_c)^{1/2}} \begin{cases} \left(\dfrac{\nu}{\nu_m}\right)^{1/3}, & \nu < \nu_m < \nu_c, \\ \left(\dfrac{\nu}{\nu_c}\right)^{1/3}, & \nu < \nu_c < \nu_m, \\ \left(\dfrac{\nu}{\nu_m}\right)^{(1-p)/2}, & \nu_m < \nu < \nu_c, \\ 1, & \nu_c < \nu < \nu_m, \\ \left(\dfrac{\nu}{\nu_m}\right)^{(1-p)/2}, & \nu_m < \nu_c < \nu, \\ \left(\dfrac{\nu}{\nu_m}\right)^{(1-p)/2}, & \nu_c < \nu_m < \nu. \end{cases} \tag{60}$$

It agrees with the usual afterglow description (e.g., Sari et al. 1998).

After the deceleration radius, we have for an adiabatic blast wave $\Gamma^2 mc^2 = E_{\rm ej}$ and then

$$F_\nu(R) = \frac{E_{\rm ej}(1+z)}{2\pi D^2 c^2}\frac{\delta L_\nu^{\max}}{\delta m} g_\nu \approx 0.3(1+z)\left(\frac{E_{\rm ej}}{10^{53}\ {\rm ergs}}\right)\left(\frac{D}{10^{28}\ {\rm cm}}\right)^{-2}\left(\frac{\epsilon_B n_0}{\mu_e}\right)^{1/2} g_\nu\ {\rm Jy}. \tag{61}$$

One can see from this equation that the observed flux at a fixed ν scales as $n_0^{1/2} g_\nu$. It can be found as a function of observer time $t_{\rm obs}$ using the approximate relation $t_{\rm obs} \approx (R/2\Gamma^2 c)(1+z)$ and the deceleration law for an adiabatic blast wave, $\Gamma^2 = E_{\rm ej}/mc^2$, which gives

$$t_{\rm obs} \approx \frac{Rmc}{2E_{\rm ej}}(1+z). \tag{62}$$

5.2. *Pair-loaded Afterglow*

We now calculate the instantaneous luminosity of the blast wave $L_\nu(\tilde{R})$ taking into account $e^\pm$ loading. The pairs dominate the material with Lagrangian coordinate $m < m_{\rm load}$. The luminosity from this material can be written as

$$L_\nu^\pm(\tilde{R}) = \int_0^{m_1} \frac{\delta L_\nu}{\delta m}\,\delta m, \quad m_1 = \min\{m_{\rm load},\ \tilde{m}\}. \tag{63}$$

At radii $\tilde{R} < R_{\rm load}$ ($\tilde{m} < m_{\rm load}$) the whole blast is $e^\pm$ dominated and its total luminosity $L_\nu = L_\nu^\pm$. At radii $\tilde{R} > R_{\rm load}$ ($\tilde{m} > m_{\rm load}$) the total luminosity is a sum of two parts: $L_\nu^\pm$ from small $m < m_{\rm load}$ and luminosity L_ν^0 from the $e^\pm$-free material $m_{\rm load} < m < \tilde{m}$. The latter peaks near $\tilde{m}$ (§ 5.1).

The total luminosity can be written as the sum

$$L_\nu = L_\nu^\pm + L_\nu^0. \tag{64}$$

At small radii $\tilde{R} < R_{\rm load}$ we have just one integral $L_\nu = L_\nu^\pm$; however, L_ν^0 may be formally kept in equation (64) and interpreted as a luminosity that would be obtained at $Z = \gamma = 1$. It would not change L_ν because $L_\nu^0 \ll L_\nu^\pm$ at $\tilde{R} < R_{\rm load}$ in the soft bands of interest.

5.2.1. *Calculation of $L_\nu^\pm$*

Pair-loaded blast waves have a special feature: the peak synchrotron frequency $\nu_m(m,\ \tilde{R})$ varies enormously with the Lagrangian coordinate m at $m < m_{\rm load}$ (see an example in Fig. 8). The peak frequency is given by

$$\tilde{\nu}_m(m) \equiv \nu_m\big(m,\ \tilde{R}\big) = 0.2\tilde{\Gamma}\frac{e\tilde{B}}{m_e c}\tilde{\gamma}_m^2 = 4.6\times 10^{12}\frac{\tilde{\Gamma}^3\Gamma\tilde{n}_0\tilde{\epsilon}_B^{1/2}\psi^2\mu_e^{5/2}}{\tilde{\gamma}\big(1+\tilde{\beta}\big)[\gamma(1+\beta)]^{3/2}Z^2 n_0^{1/2}}\ {\rm Hz}, \tag{65}$$

where we have taken into account the adiabatic cooling factor A (§ 3.2) and assumed a slow radiative cooling of $e^\pm$. The factor $\gamma^{-3/2}Z^{-2}$ appearing in this expression is a very steep function of m, $R(m)$, or $\xi(R)$, whichever is chosen as a Lagrangian coordinate in the blast wave. It varies by 5 orders of magnitude when ξ varies from $\xi_{\rm acc}/2$ to $2\xi_{\rm acc}$, which corresponds to a narrow range of R from $R_{\rm acc}/\sqrt{2}$ to $\sqrt{2}R_{\rm acc}$.

The steep variation of $\tilde{\nu}_m$ with m implies that a narrow mass shell $\Delta m \sim m_{\rm acc}$ dominates $L_\nu^\pm$ in a broad range of ν. This fact enables a simple estimate of $L_\nu^\pm$. To a first approximation, the number of $e^\pm$ whose emission peaks at a given ν does not depend on ν and equals the number of particles in the shell $\Delta m \sim m_{\rm acc}$,

$$N_* \sim Z_{\rm acc}\frac{m_{\rm acc}}{\mu_e m_p} = 74\frac{m_{\rm acc}}{m_p}. \tag{66}$$

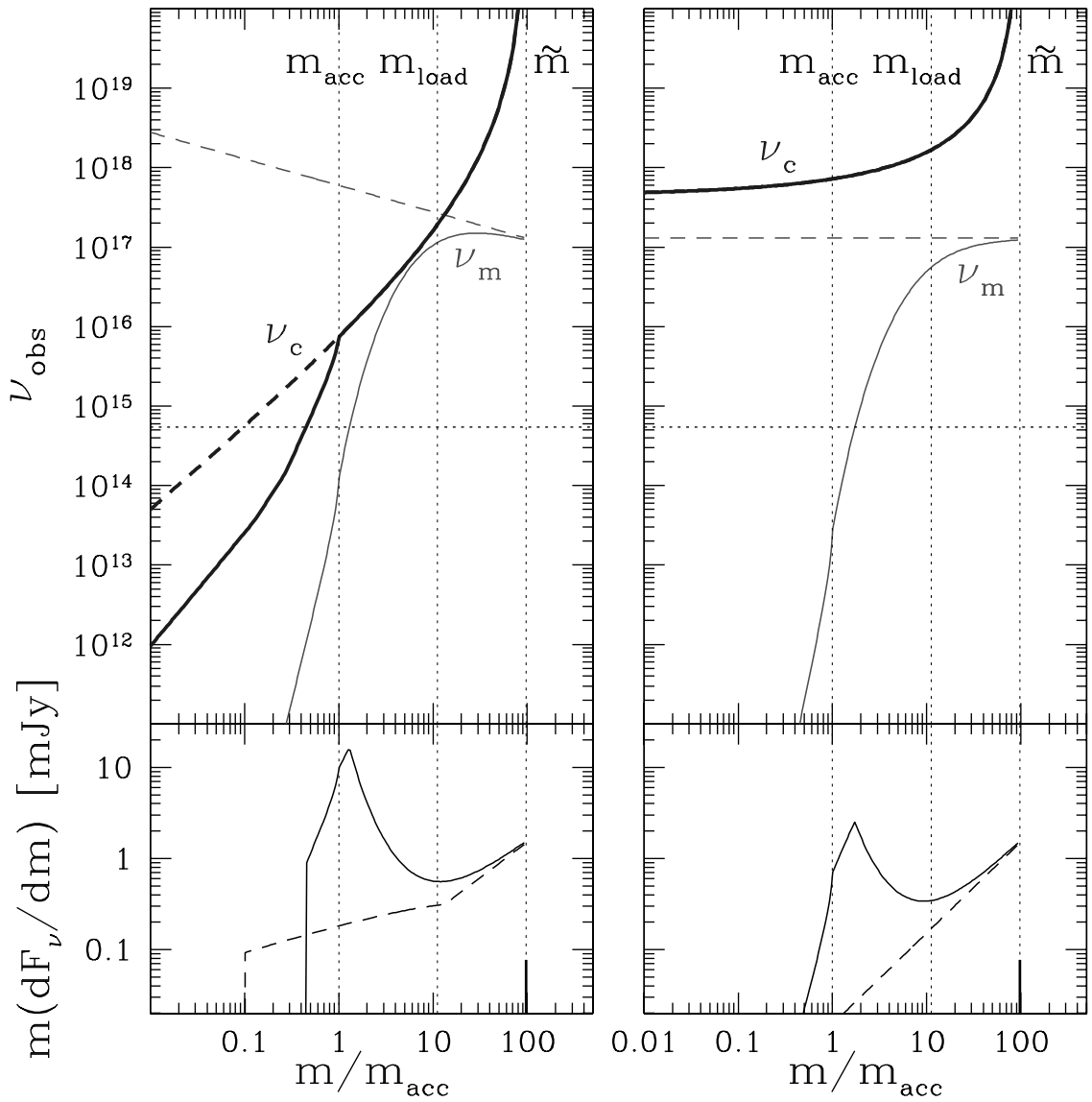

FIG. 8.—Instantaneous blast wave emission as a function of Lagrangian coordinate m at radius $\tilde{R} = R_{\rm dec}$. The blast wave model is the same as in Fig. 3. The results that would be obtained without the γ-ray front effect ($Z = 1$ and $\gamma = 1$) are shown by dashed lines. *Top*: Observed synchrotron peak frequency $\nu_m(m,\ R_{\rm dec})$ and cutoff frequency $\nu_c(m,\ R_{\rm dec})$ corrected for cosmological redshift (i.e., divided by $1+z$). The horizontal dotted line indicates the R-band frequency $\nu_{\rm obs} = 5.45\times10^{14}$ Hz. *Bottom*: Distribution of the produced optical flux over m. The emission from the $e^{\pm}$-loaded mass $m < m_{\rm load}$ sharply peaks near $m_{\rm acc}$, at a specific m_* where $\tilde{\nu}_m/(1+z) = \nu_{\rm obs}$. The pair-free emission component peaks at the current position of the shock $m = \tilde{m} = m_{\rm dec}$. *Left*: Conservation of postshock magnetic flux is assumed. *Right*: $\epsilon_B(m,\ \tilde{R}) = {\rm const} = \epsilon_B$ is assumed. [*See the electronic edition of the Journal for a color version of this figure.*]

The produced luminosity $dL^{\pm}/d\log\nu$ approximately equals $\dot{E}N_*/2$, which gives the spectral luminosity

$$L_\nu^{\pm}(\tilde{R}) = \frac{5}{12\pi}\frac{m_e c^2\sigma_{\rm T}}{e}\frac{\tilde{B}_{\rm acc}}{\tilde{\Gamma}}N_* = 30\left(\frac{\tilde{\epsilon}_{B{\rm acc}}\tilde{n}_0}{\mu_e}\right)^{1/2} Z_{\rm acc} m_{\rm acc} f_\nu, \quad \tilde{R} > R_{\rm acc}. \quad (67)$$

Here $\tilde{B}_{\rm acc}$ is the current magnetic field in the shell Δm and $\tilde{\epsilon}_{B{\rm acc}}$ is the corresponding magnetic parameter ($\tilde{B}_{\rm acc}^2/8\pi$ divided by the current energy density of the blast wave). In the first approximation, $f_\nu = 1$, i.e., $L_\nu^{\pm}$ does not depend on ν and the spectral index of emission $\alpha \approx 0$.

Calculation of $L_\nu^{\pm}$ by accurate integration over m gives the correction factor f_ν and confirms that $f_\nu \sim 1$ in a broad range of frequencies. The correction factor is derived analytically in the Appendix and shown in Figure 9. It is conveniently expressed

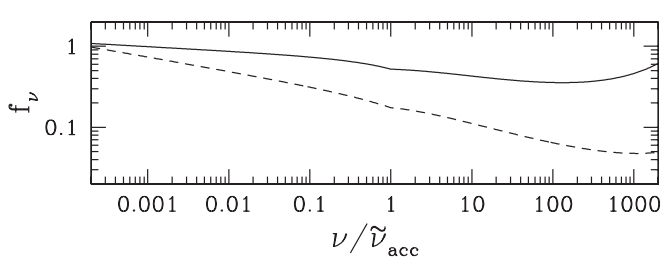

FIG. 9.—Correction factor f_ν (with $\tilde{\epsilon}_{B*} = \tilde{\epsilon}_{B{\rm acc}}$; see the Appendix). The solid line shows the case of $k = 3$ (uniform medium), and the dashed line $k = 1$ (wind-type medium). The characteristic frequency $\tilde{\nu}_{\rm acc}$ is given by equation (68).

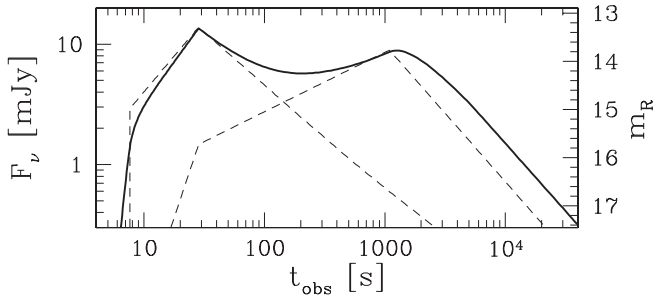

FIG. 10.—Optical light curve calculated numerically in Fig. 3 here compared with the two components $F_\nu^{\pm}$ and F_ν^0 calculated analytically (*dashed lines*).

as a function of $\nu/\tilde{\nu}_{\rm acc}$, where $\tilde{\nu}_{\rm acc} \equiv \nu_{\rm acc}(\tilde{R}) \equiv \nu_m(m_{\rm acc},\ \tilde{R})$ (thus, $\tilde{\nu}_{\rm acc}$ describes the peak of synchrotron emission from material shocked at $R = R_{\rm acc}$ after it expanded to the current $\tilde{R}$),

$$\tilde{\nu}_{\rm acc} = 4\times10^{14}\tilde{\Gamma}_2^2\left[\frac{\tilde{\Gamma}}{\Gamma(R_{\rm acc})}\right]\left[\frac{\tilde{n}_0}{n_0(R_{\rm acc})}\right]^{1/2} \times\left(\frac{\tilde{n}_0\tilde{\epsilon}_{B\rm acc}}{0.01}\right)^{1/2}\left(\frac{\psi}{0.1}\right)^2 {\rm Hz},\quad \tilde{R}\geq R_{\rm acc}. \tag{68}$$

This frequency is near the optical band.

The basic reason for the small slope α is the steep dependence of the pair-loading process on radius (the big power 17/2 appears in the problem).

5.2.2. $e^{\pm}$ *Contribution to the Observed Luminosity*

The total observed flux of the blast wave radiation is (see eqs. [46] and [64])

$$F_\nu = F_\nu^{\pm} + F_\nu^0 = \frac{(1+z)\tilde{\Gamma}^2}{3\pi D^2}\left(L_\nu^{\pm} + L_\nu^0\right), \tag{69}$$

where the pair-dominated part is given by equation (67) and the pair-free part by equation (59). This analytical result is compared with the numerical calculations in Figure 10. The analytical calculation of $F_\nu^{\pm}$ is more accurate because the integral peaks in a narrow and well-defined region of m. The standard pair-free part is still reasonably well approximated and we can compare the two components analytically.

Using equations (59) and (67), we get

$$\frac{F_\nu^{\pm}}{F_\nu^0}\left(\tilde{R}\right) = 74\mu_e\frac{m_{\rm acc}}{\tilde{m}}\frac{f_\nu}{g_\nu}\left(\frac{\tilde{\epsilon}_{B\rm acc}}{\epsilon_B}\right)^{1/2},\quad \tilde{R}\geq R_{\rm acc}. \tag{70}$$

F_ν^0 peaks in the X-ray band during the early afterglow, and $g_\nu \ll 1$ in IR, optical, and UV bands. By contrast, $F_\nu^{\pm}$ has the spectral factor $f_\nu \sim 1$ in a broad range of soft frequencies from IR to soft X-rays (§ 5.2.2).

The $e^{\pm}$-loaded material dominates the observed flux in the soft bands for two reasons: (1) the number of emitting particles is increased by the factor $Z \sim Z_{\rm acc} = 74\mu_e$ and (2) their synchrotron peak frequency is shifted to soft bands (because the mean energy per postshock particle is reduced). In addition, $\tilde{\epsilon}_{B\rm acc} > \epsilon_B$ if the postshock magnetic flux is conserved in the blast wave (see § 3.2). As a result, $F_\nu^{\pm} \gg F_\nu^0$ even when the blast wave expands to $\tilde{R} > R_{\rm load}$ where the $e^{\pm}$-loaded fraction of the blast material is very small, $m_{\rm load} \ll \tilde{m}$.

6. BLAST WAVE IN A UNIFORM MEDIUM

We now consider in detail the case of a uniform hydrogen medium, $n_0(R) = {\rm const}$ ($k = 3$) with $\mu_e = 1$ and aim to find the observed flux $F_\nu = F_\nu^{\pm} + F_\nu^0$ as a function of $t_{\rm obs}$ and $\nu_{\rm obs}$. We assume $R_{\rm load} < R_{\rm dec}$, where

$$R_{\rm dec} = \left(\frac{3E_{\rm ej}}{4\pi\Gamma_0^2 n_0 m_p c^2}\right)^{1/3} = 1.17\times10^{17}\left(\frac{E_{\rm ej}}{10^{53}\ {\rm ergs}}\right)^{1/3}\left(\frac{\Gamma_0}{100}\right)^{-2/3} n_0^{-1/3}\ {\rm cm}. \tag{71}$$

We also assume that the blast wave is approximately adiabatic and its Lorentz factor is given by

$$\tilde{\Gamma} = \Gamma_0\begin{cases} 1, & \tilde{R} < R_{\rm dec}, \\ \left(\dfrac{\tilde{R}}{R_{\rm dec}}\right)^{-3/2}, & \tilde{R} > R_{\rm dec}. \end{cases} \tag{72}$$

The approximate relation between the observer time $t_{\rm obs}$, the blast wave radius $\tilde{R}$, and its Lorentz factor $\tilde{\Gamma}$ reads (see § 4)

$$\tilde{R}(t_{\rm obs}) \approx 2\tilde{\Gamma}^2 c\frac{t_{\rm obs}}{1+z} = \begin{cases} 2\Gamma_0^2 c\left(\dfrac{t_{\rm obs}}{1}+z\right), & t_{\rm obs} < t_{\rm dec}, \\ R_{\rm dec}\left(\dfrac{t_{\rm obs}}{t_{\rm dec}}\right)^{1/4}, & t_{\rm obs} > t_{\rm dec}, \end{cases} \tag{73}$$

where

$$t_{\rm dec} = (1+z)\frac{R_{\rm dec}}{2\Gamma_0^2 c} \approx 194(1+z)\left(\frac{E_{\rm ej}}{10^{53}\ {\rm ergs}}\right)^{1/3}\left(\frac{\Gamma_0}{100}\right)^{-8/3} n_0^{-1/3}\ {\rm s} \tag{74}$$

is the deceleration time. We use below the following explicit relations at $\tilde{R} > R_{\rm dec}$:

$$\tilde{R}(t_{\rm obs}) = 3.1\times10^{16}\left(\frac{E_{\rm ej}}{10^{53}\ {\rm ergs}}\right)^{1/4} n_0^{-1/4}\left(\frac{t_{\rm obs}}{1+z}\right)^{1/4}\ {\rm cm}, \tag{75}$$

$$\tilde{\Gamma}(t_{\rm obs}) = \Gamma_0\left(\frac{t_{\rm obs}}{t_{\rm dec}}\right)^{-3/8} = 720\left(\frac{E_{\rm ej}}{10^{53}\ {\rm ergs}}\right)^{1/8} n_0^{-1/8}\left(\frac{t_{\rm obs}}{1+z}\right)^{-3/8}. \tag{76}$$

If the postshock magnetic flux is conserved in the expanding blast wave, the evolution of ϵ_B is described by equation (18),

$$\epsilon_B(m,\ \tilde{R}) = \epsilon_B\left(\frac{\tilde{\Gamma}^2}{\Gamma_0\Gamma_{\rm rel}}\right)^{1/2}\left(\frac{\tilde{R}}{R}\right)^2 = \epsilon_B[\gamma(1+\beta)]^{1/2}\begin{cases}\left(\dfrac{t_{\rm obs}}{t_{\rm dec}}\right)^2, & t_{\rm obs} < t_{\rm dec}, \\ \left(\dfrac{t_{\rm obs}}{t_{\rm dec}}\right)^{1/8}, & t_{\rm obs} > t_{\rm dec}, \end{cases} \tag{77}$$

where ϵ_B is the magnetic parameter immediately behind the shock when the blast wave had radius $R(m)$ and $\beta(m)$ is the preshock medium velocity at that moment.

6.1. *Pair-free Part*

The $e^{\pm}$-free afterglow is described by equations (46) and (59),

$$F_\nu^0 = \frac{\tilde{\Gamma}^2(1+z)}{3\pi D^2} L_\nu^0 = 10(\epsilon_B n_0)^{1/2} g_\nu \tilde{m} \tilde{\Gamma}^2 \frac{(1+z)}{\pi D^2}, \quad (78)$$

$$\tilde{m} = \frac{4\pi}{3} \tilde{R}^3 n_0 m_p. \quad (79)$$

We focus here on low frequencies $\nu < \nu_c,\ \nu_m$ and keep only the first two lines in the general expression for g_ν (eq. [60]). Substituting equations (55) and (54) for ν_m and ν_c and using $a \approx 1$ (§ 5.1), one gets

$$g_\nu \approx \begin{cases} \left(\dfrac{\nu}{\nu_m}\right)^{1/3} = 0.013 \nu_{15}^{1/3} \tilde{\Gamma}_2^{-4/3} (\epsilon_B n_0)^{-1/6} \psi^{-2/3}, & \nu < \nu_m < \nu_c, \\ \left(\dfrac{\nu}{\nu_c}\right)^{1/3} = 0.48 \nu_{15}^{1/3} \tilde{R}_{16}^{2/3} (\epsilon_B n_0)^{1/2}, & \nu < \nu_c < \nu_m. \end{cases} \quad (80)$$

Note that $\nu = (1+z)\nu_{\rm obs}$ in all the formulae. Substitution of $\tilde{R}(t_{\rm obs})$ and $\tilde{\Gamma}(t_{\rm obs})$ gives F_ν^0 as a function of $t_{\rm obs}$.

In particular, at $t_{\rm obs} < t_{\rm dec}$ we have $\tilde{\Gamma} = \Gamma_0 = {\rm const}$ and get

$$\frac{F_\nu^0}{\rm Jy} = \frac{0.3}{D_{28}^2} \left(\frac{\nu_{\rm obs}}{10^{15}\ {\rm Hz}}\right)^{1/3} \times \begin{cases} 10^{-9} \left(\dfrac{\Gamma_0}{100}\right)^{20/3} n_0^{4/3} \epsilon_B^{1/3} \psi^{-2/3} (1+z)^{-5/3} t_{\rm obs}^3, & \nu < \nu_m < \nu_c, \\ 10^{-8} \left(\dfrac{\Gamma_0}{100}\right)^{28/3} n_0^2 \epsilon_B (1+z)^{-7/3} t_{\rm obs}^{11/3}, & \nu < \nu_c < \nu_m. \end{cases} \quad (81)$$

At $t_{\rm obs} > t_{\rm dec}$, we have for an adiabatic blast wave $\tilde{\Gamma}^2 \tilde{m} c^2 = E_{\rm ej} = {\rm const}$ and rewrite F_ν as

$$F_\nu = 0.3(1+z) \left(\frac{E_{\rm ej}}{10^{53}\ {\rm ergs}}\right) D_{28}^{-2} (n_0 \epsilon_B)^{1/2} g_\nu\ {\rm Jy}, \quad (82)$$

which gives

$$\frac{F_\nu^0}{\rm Jy} = \frac{0.3}{D_{28}^2} \left(\frac{\nu_{\rm obs}}{10^{15}\ {\rm Hz}}\right)^{1/3} \times \begin{cases} 10^{-3} \left(\dfrac{E_{\rm ej}}{10^{53}}\right)^{5/6} n_0^{1/2} \epsilon_B^{1/3} \psi^{-2/3} (1+z)^{5/6} t_{\rm obs}^{1/2}, & \nu < \nu_m < \nu_c, \\ \left(\dfrac{E_{\rm ej}}{10^{53}}\right)^{7/6} n_0^{5/6} \epsilon_B (1+z)^{7/6} t_{\rm obs}^{1/6}, & \nu < \nu_c < \nu_m. \end{cases} \quad (83)$$

Here $t_{\rm obs}$ is in seconds and n_0 is in cm^{-3}; ψ is given by equation (56). The same results were derived previously (e.g., Sari et al. 1998; Panaitescu & Kumar 2000).

6.2. *Pair-dominated Part*

The characteristic frequency $\tilde{\nu}_{\rm acc}(t_{\rm obs})$ is given by

$$\tilde{\nu}_{\rm acc} = 4\times 10^{14} \left(\frac{\Gamma_0}{100}\right)^2 \left(\frac{\epsilon_{B\rm acc} n_0}{0.01}\right)^{1/2} \left(\frac{\psi}{0.1}\right)^2 \times \begin{cases} 1 & t_{\rm obs} < t_{\rm dec} \\ \left(\dfrac{t_{\rm obs}}{t_{\rm dec}}\right)^{-9/8} & t_{\rm obs} > t_{\rm dec} \end{cases} {\rm Hz}. \quad (84)$$

We have $f_\nu \sim {\rm const}$ in a broad range of frequencies around $\tilde{\nu}_{\rm acc}$ (see § 5.2.2), and therefore

$$L_\nu^{\pm} \approx ({\rm const}) \tilde{\epsilon}_{B\rm acc}^{1/2}. \quad (85)$$

The observed flux is given by

$$\frac{F_\nu^{\pm}}{\rm Jy} = \frac{\tilde{\Gamma}^2(1+z)}{2\pi D^2} L_\nu^{\pm} = 1.7\times 10^2 (1+z) \frac{R_{\rm acc}^3}{D^2} n_0^{3/2} \tilde{\epsilon}_{B\rm acc}^{1/2} \tilde{\Gamma}^2 f_\nu, \quad (86)$$

where we have used

$$m_{\rm acc} = \frac{4\pi}{3} R_{\rm acc}^3 n_0 m_p \quad (87)$$

and $R_{\rm acc}$ is given by equation (10). Finally, we substitute equation (76) for $\tilde{\Gamma}(t_{\rm obs})$ and find

$$\frac{F_\nu^{\pm}}{\rm Jy} = 1.7\times 10^{-2} (1+z) \left(\frac{\Gamma_0}{100}\right)^2 \left(\frac{R_{\rm acc}}{10^{16}\ {\rm cm}}\right)^3 \left(\frac{D}{10^{28}\ {\rm cm}}\right)^{-2} \times n_0^{3/2} f_\nu \tilde{\epsilon}_{B\rm acc}^{1/2} \begin{cases} 1, & t_{\rm obs} < t_{\rm dec}, \\ \left(\dfrac{t_{\rm obs}}{t_{\rm dec}}\right)^{-3/4}, & t_{\rm obs} > t_{\rm dec}. \end{cases} \quad (88)$$

Equation (88) shows that before $t_{\rm dec}$ the observed flux evolves as $F_\nu^{\pm}(t_{\rm obs}) = ({\rm const}) f_\nu \tilde{\epsilon}_{B\rm acc}^{1/2}$, where f_ν changes very slowly while $\tilde{\epsilon}_{B\rm acc}^{1/2}$ increases as $t_{\rm obs}$ if the postshock magnetic flux is conserved (eq. [77]) and reaches $(R_{\rm dec}/R_{\rm acc})\epsilon_B^{1/2}$ at $t_{\rm obs} = t_{\rm dec}$. After $t_{\rm dec}$, the observed flux decreases as $\tilde{\epsilon}_{B\rm acc}^{1/2} \tilde{\Gamma}^2 f_\nu$ with $\tilde{\epsilon}_{B\rm acc}^{1/2} \approx {\rm const} = (R_{\rm dec}/R_{\rm acc})\epsilon_B^{1/2}$; then

$$F_\nu^{\pm} \propto \tilde{\Gamma}^2 f_\nu \propto \left(\frac{t_{\rm obs}}{t_{\rm dec}}\right)^{-3/4-(9/8)\alpha}, \quad (89)$$

where $\alpha \sim 0.2$ is the slope of spectral function f_ν, and we get the approximate decay rate $F_\nu^{\pm} \propto t_{\rm obs}^{-0.9}$. A faster decay of $F_\nu^{\pm}$ is possible only if the magnetic field is destroyed in the blast wave and $\epsilon_{B\rm acc}$ decreases with $\tilde{R}$.

6.3. *Radiative Cooling of $e^{\pm}$*

The above analytical calculation of $F_\nu^{\pm}$ assumed that the pairs are slowly cooling. We now check this assumption.

6.3.1. *The Cooling Cutoff of the Pair Distribution*

The radiative cooling defines the cutoff of the $e^{\pm}$ distribution $\gamma_c(m,\ \tilde{R})$ (§ 3.3) and the corresponding cutoff frequency of the synchrotron spectrum $\nu_c(m,\ \tilde{R})$,

$$\nu_c(m,\ \tilde{R}) = 0.2\tilde{\Gamma} \frac{e\tilde{B}}{m_e c} \gamma_c^2(m,\ \tilde{R}), \quad (90)$$

where $\tilde{\Gamma}$ is the current Lorentz factor of the blast wave and $\tilde{B} = B(m,\ \tilde{R})$. The radiative cooling does not affect $L_\nu^{\pm}(\tilde{R})$ if $\gamma_c(m,\ \tilde{R}) > \gamma_m(m,\ \tilde{R})$ at $m \sim m_{\rm acc}$.

Both synchrotron and inverse Compton losses can affect the value of γ_c at $m_{\rm acc}$. They are proportional to the magnetic energy density $U_B(m_{\rm acc},\ \tilde{R})$ and soft radiation density $U_s(m_{\rm acc},\ \tilde{R})$, respectively.

As the blast wave expands from $R_{\rm acc}$ to some $\tilde{R} < R_{\rm dec}$, its energy density $\tilde{U}$ remains approximately constant while $\tilde{\epsilon}_{B\rm acc}$ grows as $(\tilde{R}/R_{\rm acc})^2$ (assuming that the magnetic flux is conserved; see

eq. [77]), so $U_B(m_{\rm acc},\ \tilde{R}) \approx (\tilde{R}/R_{\rm acc})^2 \epsilon_B \tilde{U}$. The expression $U_s(m_{\rm acc},\ \tilde{R})$ is dominated by synchrotron radiation transported from the forward shock, which is in the fast-cooling regime. The density of synchrotron radiation at the current position of the shock is $U_s(\tilde{m},\ \tilde{R}) \approx (\epsilon_e \epsilon_B)^{1/2} \tilde{U}$ (the rest of electron energy is taken away by inverse Compton scattering of synchrotron radiation; e.g., Sari & Esin 2001). A fraction $\sim$0.2 of this radiation is transported to the downstream region of the blast wave.[9] Then the density of soft radiation at $m \sim m_{\rm acc}$ is

$$U_s\left(m_{\rm acc},\ \tilde{R}\right) \approx 0.2(\epsilon_e \epsilon_B)^{1/2} \tilde{U}. \tag{91}$$

This implies that $U_s(m_{\rm acc},\ \tilde{R})$ is approximately constant $\tilde{R} < R_{\rm dec}$.

So, we find that the relative contribution of inverse Compton scattering to the cooling rate at $m \sim m_{\rm acc}$ is given by

$$C\left(m_{\rm acc},\ \tilde{R}\right) = \frac{U_s\left(m_{\rm acc},\ \tilde{R}\right)}{U_B\left(m_{\rm acc},\ \tilde{R}\right)} \approx 0.2 \frac{(\epsilon_e \epsilon_B)^{1/2}}{\tilde{\epsilon}_{B\rm acc}} = 0.2 \left(\frac{R_{\rm acc}}{\tilde{R}}\right)^2 \left(\frac{\epsilon_e}{\epsilon_B}\right)^{1/2}, \tag{92}$$

where the last equality assumes conservation of magnetic flux. Below we consider blast waves with $C(m_{\rm acc},\ R_{\rm dec}) \lesssim 1$; then the cutoff at $m \sim m_{\rm acc}$ is shaped by synchrotron losses rather than inverse Compton scattering of the forward shock radiation.

The cooling peaks at the deceleration radius and shapes the cutoff of the $e^{\pm}$ spectrum,

$$\gamma_c(m,\ R_{\rm dec}) = \frac{3m_e}{16 m_p \sigma_{\rm T} \tilde{\epsilon}_B n_0 \tilde{\Gamma}(R_{\rm dec} - R)} = \frac{9.62\times10^{-4} \epsilon_B^{-1} \Gamma_0}{[\gamma(1+\beta)]^{1/2}} \left(\frac{R}{10^{16}\ {\rm cm}}\right)^2 \left(\frac{E_{\rm ej}}{10^{53}\ {\rm ergs}}\right)^{-1} \times \left(1 - \frac{R}{R_{\rm dec}}\right)^{-1}, \tag{93}$$

$$\nu_c(m,\ R_{\rm dec}) = 3.25\times10^{15} \left[\frac{\epsilon_B(m,\ R_{\rm dec}) n_0}{0.01}\right]^{-3/2} \times \left(\frac{R_{\rm dec}}{10^{17}\ {\rm cm}}\right)^{-2} \left(1 - \frac{R}{R_{\rm dec}}\right)^{-2} {\rm Hz} = \frac{3.25\times10^{15}}{[\gamma(1+\beta)]^{3/4}} \left(\frac{\epsilon_B n_0}{0.01}\right)^{-3/2} \left(\frac{m}{m_{\rm dec}}\right) \times \left(\frac{R_{\rm dec}}{10^{17}\ {\rm cm}}\right)^{-2} \left(1 - \frac{R}{R_{\rm dec}}\right)^{-2} {\rm Hz}, \tag{94}$$

where $R \approx R_{\rm acc}$ is the radius where the pair-loaded mass $m \sim m_{\rm acc}$ was shocked and $\gamma(1+\beta)$ is the preacceleration factor at this radius. The last equalities in these expressions assume magnetic flux conservation. In particular, the factors $m/m_{\rm dec}$ and $[\gamma(1+\beta)]^{-3/4}$ appeared in the expression for $\nu_c(m,\ R_{\rm dec})$ because of the flux conservation; they would be absent if $\epsilon_B(m,\ \tilde{R}) = {\rm const}$.

When the blast wave reaches the deceleration radius, its pressure starts to decrease, and the afterward evolution of the $e^{\pm}$ distribution function at $m \sim m_{\rm acc}$ is fully determined by adiabatic cooling: radiative cooling is slower and has a negligible effect. The adiabatic cooling of the blast wave expanded from $R_{\rm dec}$ to a current $\tilde{R}$ is described by the factor $A = (\tilde{\Gamma}/\Gamma_0)^{1/2}$ (§ 3.3), and the resulting cutoff Lorentz factor is

$$\gamma_c\left(m,\ \tilde{R}\right) = \left(\frac{\tilde{\Gamma}}{\Gamma_0}\right)^{1/2} \gamma_c(m,\ R_{\rm dec}), \quad \tilde{R} > R_{\rm dec}. \tag{95}$$

The corresponding cutoff frequency evolves as $\tilde{\nu}_c \propto \tilde{\Gamma} \tilde{B} \tilde{\gamma}_c^2$, which gives

$$\frac{\nu_c\left(m,\ \tilde{R}\right)}{\nu_c(m,\ R_{\rm dec})} = \left(\frac{\tilde{\Gamma}}{\Gamma_0}\right)^3 \left[\frac{\epsilon_B\left(m,\ \tilde{R}\right)}{\epsilon_B(m,\ R_{\rm dec})}\right]^{1/2}, \quad \tilde{R} > R_{\rm dec}. \tag{96}$$

It can be expressed as a function of $t_{\rm obs}$ using equation (76) for $\tilde{\Gamma}$ and a prescription for the magnetic field evolution in the blast wave. If the magnetic flux is conserved, $\tilde{\epsilon}_B^{1/2}$ evolves as $t_{\rm obs}^{1/16}$ (eq. [77]), and we get

$$\frac{\nu_c(m,\ t_{\rm obs})}{\nu_c(m,\ t_{\rm dec})} = \left(\frac{t_{\rm obs}}{t_{\rm dec}}\right)^{-9/8+1/16} \approx \left(\frac{t_{\rm obs}}{t_{\rm dec}}\right)^{-17/16}, \quad t_{\rm obs} > t_{\rm dec}. \tag{97}$$

If ϵ_B remained constant at all m and $\tilde{R}$, one gets the cutoff frequency $\nu_c(m,\ t_{\rm obs}) \propto t_{\rm obs}^{-9/8}$, almost the same as with flux conservation.

6.3.2. *The Slow-Cooling Condition*

A given shell m in a blast wave of radius $\tilde{R}$ is in the slow cooling regime if $\gamma_c(m,\ \tilde{R}) > \gamma_m(m,\ \tilde{R})$. Using equation (22),

$$\gamma_m\left(m,\ \tilde{R}\right) = \frac{\Gamma}{Z\gamma(1+\beta)} \psi \frac{m_p}{m_e}, \tag{98}$$

we find with the flux conservation assumption

$$\left[\frac{\nu_m(m,\ R_{\rm dec})}{\nu_c(m,\ R_{\rm dec})}\right]^{1/2} = \frac{\gamma_m(m, R_{\rm dec})}{\gamma_c(m, R_{\rm dec})} = \frac{1.91\times10^6 \epsilon_B \psi}{Z[\gamma(1+\beta)]^{1/2}} \left(\frac{R}{10^{16}\ {\rm cm}}\right)^{-2} \times \left(\frac{E_{\rm ej}}{10^{53}\ {\rm ergs}}\right) \left(1 - \frac{R}{R_{\rm dec}}\right). \tag{99}$$

Note that n_0 and Γ_0 cancel out from this expression. This ratio remains the same at $\tilde{R} > R_{\rm dec}$ as both $\gamma_m(m,\ R_{\rm dec})$ and $\gamma_c(m,\ R_{\rm dec})$ evolve adiabatically and are reduced by a common factor A. The effect of the γ-ray precursor enters through the factor $Z^{-1}[\gamma(1+\beta)]^{-1/2}$, which reduces the ratio.

We are interested in $m \approx m_{\rm acc}$ because $L_\nu^{\pm}$ peaks near $m_{\rm acc}$. Equation (99) shows that the slow-cooling assumption is valid if

$$\frac{1.91\times10^6 \epsilon_B \psi}{Z_{\rm acc}} \left(\frac{R_{\rm acc}}{10^{16}\ {\rm cm}}\right)^{-2} \left(\frac{E_{\rm ej}}{10^{53}\ {\rm ergs}}\right) < 1, \tag{100}$$

which can be rewritten as

$$\epsilon_B \epsilon_e < 4\times10^{-5} \left(\frac{p-1}{p-2}\right) \left(\frac{R_{\rm acc}}{10^{16}\ {\rm cm}}\right)^2 \left(\frac{E_{\rm ej}}{10^{53}\ {\rm ergs}}\right)^{-1} \approx 2\times10^{-5} \left(\frac{p-1}{p-2}\right) \left(\frac{E_\gamma}{E_{\rm ej}}\right). \tag{101}$$

[9] The transport coefficient is evaluated assuming isotropic emission from the forward shock in the blast wave frame. Its dependence on the downstream Lagrangian coordinate m is weak as long as $m \ll \tilde{m}$. For example, the contact discontinuity ($m = 0$) receives $\sim$0.15 of the forward shock emission.

7. COMPARISON WITH THE REVERSE SHOCK MODEL

We focused in this paper on the forward shock of the GRB explosion. Early optical radiation is also expected from the reverse shock in the ejecta if their energy is dominated by baryons rather than magnetic field (Mészáros & Rees 1993; Sari & Piran 1999). Explosions with the reverse and $e^{\pm}$-loaded forward shocks should have two soft emission components, and it is instructive to compare them.

Emission from the reverse shock peaks when it crosses the ejecta, which occurs at the deceleration radius. Then the explosion Lorentz factor $\tilde{\Gamma}$ decreases and the ejecta emission decays. The decay rate can be calculated as follows. The Lorentz factor of electrons emitting at a fixed frequency $\nu_{\rm obs} = (1+z)\nu$ is

$$\gamma_e = \gamma_\nu = \left(\frac{5\nu m_e c}{\tilde{\Gamma}\tilde{B}_{\rm ej}}\right)^{1/2} \propto \left(\tilde{B}_{\rm ej}\tilde{\Gamma}\right)^{-1/2}, \qquad (102)$$

where $\tilde{B}_{\rm ej}$ is the magnetic field in the ejecta at the current radius $\tilde{R}$. The number of electrons emitting at frequency ν is

$$N_\nu \approx N_e(\gamma_\nu/\gamma_m)^{-p+1}, \qquad (103)$$

where N_e is the total number of shock-accelerated electrons and $\gamma_\nu > \gamma_m$ is assumed. With decreasing $\tilde{\Gamma}$, N_ν is reduced for two reasons: (1) γ_ν increases and (2) γ_m decreases as the whole nonthermal spectrum is shifted to lower energies by adiabatic cooling. The adiabatic cooling factor is $A \propto n_{\rm ej}^{1/3} \propto \tilde{P}^{1/3\hat{\gamma}}$, where $\hat{\gamma}$ is the adiabatic index of the ejecta material and $\tilde{P} = (4/3)\tilde{\Gamma}^2\tilde{n}_0\mu_e m_p c^2$ is the blast wave pressure, and hence

$$N_\nu \propto \gamma_\nu^{-p+1}A^{p-1} \propto \left(\tilde{B}_{\rm ej}\tilde{\Gamma}\right)^{(p-1)/2}\tilde{n}_0^{(p-1)/3\hat{\gamma}}\tilde{\Gamma}^{2(p-1)/3\hat{\gamma}}. \qquad (104)$$

The observed synchrotron flux is given by

$$F_\nu^{\rm RS} = \frac{5(1+z)}{36\pi^2 D^2}\frac{m_e c^2\sigma_{\rm T}}{e}\tilde{B}_{\rm ej}\tilde{\Gamma}N_\nu \propto \tilde{n}_0^{(p-1)/3\hat{\gamma}}\tilde{B}_{\rm ej}^{(p+1)/2}\tilde{\Gamma}^{(p+1)/2+2(p-1)/3\hat{\gamma}}. \qquad (105)$$

If no destruction of magnetic flux takes place, $\tilde{B}_{\rm ej}$ evolves as

$$\tilde{B}_{\rm ej} \propto \tilde{n}_{\rm ej}\tilde{R} \propto P^{1/\hat{\gamma}}\tilde{R}. \qquad (106)$$

Then

$$F_\nu^{\rm RS} \propto \tilde{n}_0^{(5p+1)/6\hat{\gamma}}\tilde{\Gamma}^{(p+1)/2+(5p+1)/3\hat{\gamma}}\tilde{R}^{(p+1)/2}. \qquad (107)$$

In the case of a uniform ambient medium, $\tilde{n}_0 = {\rm const}$, we have after the deceleration radius $\tilde{\Gamma} \propto t_{\rm obs}^{-3/8}$ and $\tilde{R} \propto t_{\rm obs}^{1/4}$, which yields

$$F_\nu^{\rm RS} \propto t_{\rm obs}^{-(p+1)/16-(5p+1)/8\hat{\gamma}} = \begin{cases} t_{\rm obs}^{-1.2}, & \hat{\gamma} = 5/3,\ p = 2.5, \\ t_{\rm obs}^{-1.5}, & \hat{\gamma} = 4/3,\ p = 2.5. \end{cases} \qquad (108)$$

A destruction of magnetic field in the ejecta could only steepen the decay.

The mechanism of reverse shock emission is similar to that of the $e^{\pm}$ afterglow: a shell of material (ejecta in the case of reverse shock and $m_{\rm acc}$ in the case of $e^{\pm}$-loaded forward shock) is heated at $R < R_{\rm dec}$ with a low energy per particle, and after $R_{\rm dec}$ the shell cools down passively (adiabatically), producing a decaying flux of soft emission.

The main difference between the two cases is the spectrum of emitting particles. The reverse shock is thought to produce a power-law electron distribution with $p = 2$–3. By contrast, the effective spectrum of $e^{\pm}$ has $p \approx 1$. In the narrow shell $\Delta m \sim m_{\rm acc}$, there are approximately equal numbers of $e^{\pm}$ at all energies up to the cooling cutoff, which gives the effective p about unity. The flat distribution of $e^{\pm}$ leads to the slow decay of their synchrotron emission that we found in § 6. The resulting light curve can, however, be made steeper if the ambient density decreases with radius or magnetic field is gradually destroyed downstream of the shock. Therefore, the main intrinsic difference between the reverse shock and $e^{\pm}$ emission components is not the produced light curve but the slope of the $e^{\pm}$ distribution p.

This difference can be observed directly by measuring the instantaneous synchrotron spectrum. The $e^{\pm}$ radiation is expected to have a small spectral index $|\alpha| < 0.2$ while the reverse shock spectrum is much steeper: $\alpha = (p-1)/2 = 0.5$–1 for $p = 2$–3. A measurement of the instantaneous spectrum in UV, optical, or IR at $t_{\rm obs} \sim 100$ s would provide a test of the current theoretical picture of the GRB explosion. Such a test can be done by *Swift*.

Finally, we note one more difference between the reverse shock and $e^{\pm}$ emission components. Both are cut off when $\nu_c < \nu$, which happens at different times because the cooling frequencies ν_c are different in the two cases. The ejecta magnetic field is likely stronger, $B_{\rm ej} > B$; then its cooling frequency is lower by the factor $(B_{\rm ej}/B)^{-3}$, and hence the cutoff should occur sooner.

8. DISCUSSION

8.1. $e^{\pm}$ Component of GRB Afterglow

An explosion blast wave is composed of swept-up layers (shells) of external medium that have been shocked in the forward shock front. In GRB explosions, these layers contain $e^{\pm}$ pairs injected into the external medium by the γ-ray front. The layers shocked at small radii $R < R_{\rm load}$ are dominated by the $e^{\pm}$. At $R > R_{\rm load}$, these layers remain in the blast wave and form a thin $e^{\pm}$ shell adjacent to the contact discontinuity if there is no turbulent mixing in the blast. This shell has a low energy per particle and emits much softer synchrotron radiation compared to the outer swept-up material. The optical emission of the expanding blast wave can be strongly dominated by the $e^{\pm}$ shell even at large radii where its mass $m_{\rm load}$ is small compared to the total swept-up mass. If the shock magnetic parameter ϵ_B is below a critical value $\sim 10^{-3}$, the optical-emitting $e^{\pm}$ are in the slow-cooling regime and radiate their energy slowly, on a timescale longer than the deceleration time of the explosion. Their effect on the observed afterglow is described by adding a new emission component $F_\nu^{\pm}$.

The $e^{\pm}$ afterglow component is less sensitive to the model assumptions than the customary pair-free afterglow. This is because the $e^{\pm}$ shell contains approximately equal numbers of particles with vastly different energies, which is a consequence of the steep evolution of the γ-ray front and $e^{\pm}$ loading with radius. This fact allowed us to derive a simple formula for the observed spectral flux,

$$F_\nu^{\pm} = 6\times 10^{-7}\tilde{\Gamma}^2\frac{(1+z)}{D_{28}^2}\tilde{\epsilon}_{B{\rm acc}}^{1/2}n_0^{3/2}\left(\frac{E_\gamma}{10^{53}\ {\rm ergs}}\right)^{3/2} f_\nu\ {\rm Jy}. \qquad (109)$$

It depends on the blast wave Lorentz factor $\tilde{\Gamma}$ that approximately corresponds to a given observer time $t_{\rm obs}$. In a broad range of ν, the flux is dominated by a specific mass shell $m \approx m_{\rm acc}$ whose shock radius was $R_{\rm acc} = 7\times 10^{15}E_{\gamma,53}^{1/2}$ cm. The

quantity $F_\nu^\pm$ depends on the magnetic field in this mass shell, $\tilde{B}_{\rm acc}$, which we parameterize using the usual equipartition parameter $\tilde{\epsilon}_{B\rm acc}$ ($\tilde{B}_{\rm acc}^2/8\pi$ divided by the energy density of the blast wave). Accurate calculations in §§ 4 and 5 give the correction factor $f_\nu \sim 1$ in equation (109). All the details and uncertainties of the blast wave physics are absorbed by this factor (which is never much different from unity) and $\tilde{\epsilon}_{B\rm acc}$.

To the first approximation, $F_\nu^\pm$ decays after the deceleration time as $\tilde{\Gamma}^2$, which is proportional to $t_{\rm obs}^{-3/4}$ for an adiabatic blast wave in a uniform medium. The decay can, however, be faster if $B_{\rm acc}$ is gradually destroyed as the blast wave expands.

8.2. *Uncertainties in the Blast Wave Physics*

8.2.1. *Magnetic Field Downstream of the Shock*

The magnetic field behind the shock front and its downstream evolution are a major uncertainty of the current blast wave models. In this paper we assumed, as is customary, that the magnetic parameter ϵ_B immediately behind the shock front remains constant as the shock expands and followed the downstream evolution of $\epsilon_B(m, \tilde{R})$ assuming conservation of the postshock magnetic flux. This assumption unambiguously determines the magnetic field in the $e^\pm$ shell, and we found that the shell is in the slow-cooling regime if the shock parameter ϵ_B is below a critical value $\sim 10^{-3}$. If ϵ_B is above this value, the $e^\pm$ shell is in the fast-cooling regime and most of its energy is radiated at $t_{\rm obs} < t_{\rm dec}$. In this case, the $e^\pm$ radiation can be visible at $t_{\rm obs} > t_{\rm dec}$ only in the infrared band; the time of the emission cutoff depends on frequency as $\nu_{\rm obs}^{-1}$.

The results are qualitatively similar if ϵ_B does not evolve in the postshock region according to the flux conservation but instead remains constant (which requires a gradual destruction of the magnetic flux with increasing distance behind the shock). However, the results would change if the magnetic flux is destroyed more quickly. The luminosity of the $e^\pm$ shell is proportional to its magnetic field and the field destruction would give a faster decay of $F_\nu^\pm$.

A real postshock field can be inhomogeneous on small scales (Medvedev & Loeb 1999) and one may need to include a distribution $f(\epsilon_B)$ in future afterglow models. This can change details. For instance, the cooling cutoff would be less pronounced because the low-ϵ_B fraction would continue to radiate in the slow-cooling regime and give a tail of emission even when most of the postshock plasma is cooled and does not emit at the observed frequency.

8.2.2. *Turbulent Mixing*

The $e^\pm$-dominated material may not form a distinct thin shell near contact discontinuity if there are large-scale turbulent motions that mix up the postshock layers. Rayleigh-Taylor instability can drive such mixing like it does in supernova remnants. The mixing is unlikely to change the results of this paper. As long as we approximate the blast wave as a constant-pressure shell, the pressure in an $e^\pm$-dominated gas element does not depend on its position within the blast wave. Therefore, its adiabatic and radiative cooling is the same as in the absence of turbulent mixing, and conservation of magnetic flux gives the same magnetic field in the element.

8.2.3. *Mechanism of Electron Acceleration*

A significant uncertainty in the afterglow physics is the mechanism of electron acceleration. A preshock magnetic field is compressed in the relativistic shock and becomes transverse, and the fields generated by Weibel instability are also transverse—parallel to the shock plane (Medvedev & Loeb 1999). Standard diffusive acceleration is unlikely to be efficient under such conditions. It requires the electron to cross the shock front many times, which can hardly happen: the upstream diffusion across the transverse field is slow because the electron gyroradius is smaller than the front thickness (proton gyroradius), and the electron will be advected downstream with the flow velocity $c/3$ with respect to the front before it gets a chance to diffuse back to the upstream region.

An alternative mechanism is stochastic acceleration by turbulence downstream of the shock. It may not be well described as impulsive acceleration and may keep electrons energetic even in the presence of significant radiative or adiabatic losses. This could change the theoretical afterglow light curve.

However, the main signature of $e^\pm$ emission (white spectrum) will likely persist because the blast wave will still have a steep variation of $e^\pm$ density with the Lagrangian coordinate m, which invariably leads to the broad $e^\pm$ distribution with $p \approx 1$. This special feature ultimately comes from the γ-ray front evolution with radius and is not related to the mechanism of $e^\pm$ acceleration.

8.2.4. *Electron Distribution Function*

Customary afterglow calculations assume an idealized distribution function of the postshock electrons: all electrons reside in a power-law component that starts at γ_m and ends at γ_c. In reality, it is possible that only a small fraction of electrons ζ_e are accelerated in a shock wave and the rest of them form a quasi-Maxwellian distribution; this is observed to be the case for collisionless shocks in the solar system. The expected energy of the accelerated electron population ϵ_e is then typically $\sim 1\%$ of the total plasma energy (which is dominated by the hot ions). Similar electron acceleration was inferred for supernova shocks. By contrast, ϵ_e inferred from the existing fits of GRB afterglows is $\epsilon_e \sim 0.1$ (e.g., Panaitescu & Kumar 2002).

We point out that the high ϵ_e may have been inferred because the fits assume $\zeta_e = 1$. Equally good fits may be obtained with a more reasonable $\zeta_e \sim 0.1$ and $\epsilon_e \sim 0.01$. This can be understood by looking at how the parameters enter the emission model. Besides the spectral slope p, the emitting electrons are described by two parameters: the number of accelerated particles $N_e = \zeta_e N_t$ (where N_t is the total number of swept-up particles) and the minimum nonthermal Lorentz factor γ_m. Note that $\gamma_m m_e c^2$ is comparable with the mean energy per electron, which is proportional to ϵ_e/ζ_e. Relaxing the assumption $\zeta_e = 1$, one can get the same γ_m by decreasing $\epsilon_e \propto \zeta_e$, and then the same observed emission may be explained with 10 times lower, and physically more plausible, values of ζ_e and ϵ_e. The number of emitting particles N_e will not be changed if N_t is increased by the factor ζ_e^{-1}. Thus, the reduction of ζ_e implies a higher ambient density and the circumburst density may have been systematically underestimated in the afterglow fits by 1 order of magnitude.

Different assumptions concerning the shape of electron distribution function can lead to different afterglow radiation. However, the $e^\pm$ afterglow component is almost insensitive to such assumptions. For illustrative purpose, consider an extreme case. Suppose there is no power-law acceleration at the shock front, and the shock produces a narrow $e^\pm$ distribution peaking at $\gamma_e(R) \approx \epsilon_e(m_p/m_e)\Gamma(\gamma Z)^{-1}$. The factor γZ is determined by the γ-ray transfer through the ambient medium and has the robust steep dependence on R near $R_{\rm acc}$ (§ 2). Therefore, γ_e will depend steeply on R, and the resulting $e^\pm$ distribution in the shell $\Delta m \sim m_{\rm acc}$ swept-up near $R_{\rm acc}$ will be broad and flat. The same

formula (eq. [109]) will describe the $e^{\pm}$ radiation with a slightly different numerical factor $f_\nu \sim 1$.

8.3. *Prospects of Detection of $e^{\pm}$ Emission*

The $e^{\pm}$ radiation is predicted to have a special feature that can be tested with upcoming observations: its spectral index α is close to zero ($|\alpha| \lesssim 0.2$). This is a significant difference from the reverse shock model, which predicts a steeper spectrum, $\alpha = (p-1)/2$, where $p = 2$–3 is a putative slope of the electron distribution. Although the early optical emission has already been caught in a few bursts, no spectral data are presently available. *Swift* can provide the valuable spectral information.

The $e^{\pm}$ dominance of the early UV/optical/IR afterglow can result in a characteristic two-peak shape of the light curve (see an example in Fig. 3). The $e^{\pm}$ emission component begins to decay at the deceleration time (eq. [74]), which can be before *Swift* detects the afterglow. However, its decay is relatively slow ($F_\nu^{\pm} \propto \Gamma^2 \propto t_{\rm obs}^{-3/4}$ in the first approximation) and its tail is observable on timescales of minutes until the pair-free component takes over. The $e^{\pm}$ radiation should be visible for a longer time in the infrared band.

To date, early optical emission ($t_{\rm obs} < 1000$ s) has been detected in four bursts: GRB 990123, GRB 021004, GRB 021211, and GRB 030418. In only one of them, GRB 990123, the peak of the optical flash was caught (Akerlof et al. 1999). This peak overlapped with the prompt MeV burst, and hence the model developed in the present paper does not apply to GRB 990123: the $e^{\pm}$ must be Compton cooled by the MeV photons (keV in the fluid frame), and most of the $e^{\pm}$ energy is likely emitted in the GeV–TeV band (Beloborodov 2005). The strong optical $e^{\pm}$ radiation is expected in bursts where the MeV radiation front completely overtakes the blast wave by the time it reaches $R_{\rm acc}$ as discussed in § 1.

8.4. *Neutron Front*

We studied in this paper the pair-loading effects on the forward shock. If the ejecta contains baryons, i.e., is not a pure electromagnetic outflow (Poynting flux), a significant fraction of the baryons must be free neutrons (Derishev et al. 1999; Beloborodov 2003b). The neutron ejecta get completely decoupled and coast freely by the beginning of afterglow emission with a Lorentz factor $\Gamma_n \sim \Gamma_{\rm ej}$. They gradually β-decay; however, some neutrons survive until radii $R \sim 10^{17}$ cm when the blast wave may have already decelerated, overtake the blast wave, and decay ahead of it depositing significant momentum and energy into the ambient medium (Beloborodov 2003a). Thus, GRB explosions are likely to develop leading neutron fronts that change the mechanism of the blast wave.

The neutron front may emerge either after the $e^{\pm}$ loading, at $R > R_{\rm load}$, or at smaller radii, depending on the presence of fast neutrons with $\Gamma_n > \Gamma$. The impact of a fast neutron front on the early afterglow was recently studied by Fan et al. (2004), and an alternative scenario with slow neutrons was proposed by Peng et al. (2004). Accurate afterglow calculation that includes both the neutron decay and $e^{\pm}$ loading is a challenging theoretical problem that may be solved in the future. We expect the main signature of $e^{\pm}$ loading—soft emission with a broad flat spectrum—to be present in neutron-fed afterglows as well.

I am grateful to Frederic Daigne, Robert Mochkovitch, and Chris Thompson for discussions and the IAP for hospitality. I also thank Jules Halpern and Davide Lazzati, the referee, for comments on the manuscript. This work was supported by NASA grant NAG5-13382 and the Alfred P. Sloan Fellowship.

APPENDIX

CALCULATION OF $L_\nu^{\pm}$ INTEGRAL

We here calculate the integral $L_\nu^{\pm}$ neglecting the cooling cutoff of the $e^{\pm}$ distribution function (i.e., assuming $\tilde\nu_c > \nu,\ \tilde\nu_m$). Then,

$$\frac{\delta L_\nu}{\delta m} = \frac{\delta L_\nu^{\max}}{\delta m} \begin{cases} \left(\dfrac{\nu}{\tilde\nu_m}\right)^{1/3}, & \tilde\nu_m \geq \nu, \\ \left(\dfrac{\nu}{\tilde\nu_m}\right)^{(1-p)/2}, & \tilde\nu_m \leq \nu, \end{cases} \tag{A1}$$

$$\frac{\delta L_\nu^{\max}}{\delta m}(m,\ \tilde R) = w(\tilde R)\tilde\epsilon_B^{1/2}\frac{Z}{\mu_e}, \qquad w(\tilde R) = 30\left[\frac{\tilde n_0 \mu_e}{\tilde\gamma(1+\tilde\beta)}\right]^{1/2} \text{ergs g}^{-1}. \tag{A2}$$

We have written $\delta L_\nu^{\max}/\delta m$ in this form to separate quantities that do not depend on the Lagrangian coordinate (functions of the current radius $\tilde R$ only) and are constant in the $L_\nu^{\pm}$ integral. In a similar way, we rewrite the expression for $\nu_m(m,\ \tilde R)$ (eq. [65]),

$$\nu_m(m,\ \tilde R) = q(\tilde R)\frac{\tilde\epsilon_B^{1/2}\Gamma}{n_0^{1/2}[\gamma(1+\beta)]^{3/2}(Z/\mu_e)^2}, \qquad q(\tilde R) = 4.6\times10^{12}\frac{\tilde\Gamma^3\tilde n_0\mu_e^{1/2}\psi^2}{\tilde\gamma(1+\tilde\beta)} \text{ Hz}. \tag{A3}$$

Since $\tilde\nu_m(m) = \nu_m(m,\ \tilde R)$ is a monotonic function of the Lagrangian coordinate $0 < m < m_1$, we can change the integration variable to ν_m,

$$L_\nu^{\pm} = \int_0^{m_1}\frac{\delta L_\nu}{\delta m}\,dm = \int_0^{\tilde\nu_1}\frac{\delta L_\nu}{\delta m}\left(\frac{\partial\nu_m}{\partial m}\right)_{\tilde R}^{-1}d\nu_m, \tag{A4}$$

where $\tilde{\nu}_1$ is the peak frequency of synchrotron emission at m_1,

$$\tilde{\nu}_1 = \begin{cases} \nu_m(\tilde{m},\ \tilde{R}) = 4.6\times10^{12}\dfrac{\tilde{\Gamma}^4\tilde{n}_0^{3/2}}{\left[\tilde{\gamma}(1+\tilde{\beta})\right]^{5/2}\tilde{Z}^2}\epsilon_B^{1/2}\psi^2\mu_e^{5/2}\ \mathrm{Hz}, & \tilde{R}\le R_{\rm load}, \\ \nu_m(m_{\rm load},\ \tilde{R}), & \tilde{R}\ge R_{\rm load}. \end{cases} \tag{A5}$$

The partial derivative of ν_m can be written as

$$\left(\frac{\partial\nu_m}{\partial m}\right)_{\tilde{R}} = \frac{\nu_m}{m}\frac{\partial\ln\nu_m}{\partial\ln m} = \frac{\nu_m}{m}\left\{\frac{\partial}{\partial\ln m}\ln\left[\frac{\tilde{\epsilon}_B^{1/2}\Gamma}{n_0^{1/2}(1+\beta)^{3/2}}\right] - \frac{\partial}{\partial\ln m}\left(\frac{Z^2}{\mu_e^2}\gamma^{3/2}\right)\right\}. \tag{A6}$$

The quantity $Z^2\gamma^{3/2}$ varies with m much faster than $\tilde{\epsilon}_B^{1/2}\Gamma n_0^{-1/2}(1+\beta)^{-3/2}$ (in the latter, only Γ could vary significantly, but even that does not happen for explosions with $R_{\rm dec} > R_{\rm acc}$). Therefore, the second term in equation (A6) is dominant, and the first term can be neglected. Then,

$$\frac{\partial\ln\nu_m}{\partial\ln m} \approx -\frac{\partial}{\partial\ln m}\left(\frac{Z^2}{\mu_e^2}\gamma^{3/2}\right) = -\frac{\partial\ln R}{\partial\ln m}\frac{\partial\ln\xi}{\partial\ln R}\frac{d}{d\ln\xi}\left(\frac{Z^2}{\mu_e^2}\gamma^{3/2}\right) = -\frac{2}{k}\frac{d}{d\ln\xi}\left(\frac{Z^2}{\mu_e^2}\gamma^{3/2}\right). \tag{A7}$$

The expressions Z/μ_e and γ are given as functions of ξ in equations (4) and (5), and we find

$$\left(\frac{\partial\nu_m}{\partial m}\right)_{\tilde{R}} = \frac{\nu_m}{m}\frac{s}{k}\begin{cases}\dfrac{10\xi(m)}{\xi_{\rm acc}}, & m\ge m_{\rm acc}, \\ \dfrac{17}{2}, & m\le m_{\rm acc}.\end{cases} \tag{A8}$$

Using equations (A1) and (A2), we get

$$L_\nu^{\pm}(\nu,\ \tilde{R}) = w(\tilde{R})\int_0^{\tilde{\nu}_1}\tilde{\epsilon}_B^{1/2}\frac{Z}{\mu_e}\left\{\begin{array}{ll}\left(\dfrac{\nu_m}{\nu}\right)^{-1/3} & \nu_m\ge\nu \\ \left(\dfrac{\nu_m}{\nu}\right)^{(p-1)/2} & \nu_m\le\nu\end{array}\right\}\left(\frac{\partial\nu_m}{\partial m}\right)_{\tilde{R}}^{-1}d\nu_m. \tag{A9}$$

The quantity Z needs to be expressed as a function of ν_m. From equations (4) and (5),

$$\gamma = \begin{cases}1, & Z/\mu_e\le e^5/2\approx 74, \\ (2Z/e^5\mu_e)^{3/2}, & Z/\mu_e\ge e^5/2,\end{cases} \tag{A10}$$

which we substitute into equation (A3) and then express Z from that equation,

$$\frac{Z}{\mu_e} = \begin{cases}\left[\nu_m(1+\beta)^{3/2}n_0^{1/2}q^{-1}\tilde{\epsilon}_B^{-1/2}\Gamma^{-1}\right]^{-1/2}, & m(\nu_m)\ge m_{\rm acc}, \\ \left[\nu_m(1+\beta)^{3/2}n_0^{1/2}q^{-1}\tilde{\epsilon}_B^{-1/2}\Gamma^{-1}\right]^{-4/17}74^{9/17}, & m(\nu_m)\le m_{\rm acc}.\end{cases} \tag{A11}$$

The quantities n_0, $\tilde{\epsilon}_B$, and Γ vary with m and therefore vary with ν_m when ν_m is chosen as the independent variable. However, their variation with ν_m is slow (because ν_m is a steep function of m). Therefore, with sufficient accuracy, we have $Z\propto\nu_m^{-1/2}$ at $m(\nu_m) > m_{\rm acc}$ and $Z\propto\nu_m^{-4/17}$ at $m(\nu_m) < m_{\rm acc}$.

Now the integral given by equation (A9) can be calculated. We consider first $\tilde{R}\le R_{\rm acc}$ and then $\tilde{R}\ge R_{\rm acc}$.

A1. $\tilde{R}\le R_{\rm acc}$

At radii $\tilde{R} < R_{\rm acc}$ the Lagrangian coordinate $m\le\tilde{m} < m_{\rm acc}$; then $\partial\ln\nu_m/\partial\ln m = (17/k)$ and $Z\propto\nu_m^{-4/17}$.

For $\nu > \tilde{\nu}_1$ we have $\nu_m < \nu$ in the whole blast, and the integral given by equation (A9) reads

$$L_\nu^{\pm}(\nu,\ \tilde{R}) = w(\tilde{R})\frac{k}{2}\epsilon_B^{1/2}\frac{Z_1}{\mu_e}m_1\left(\frac{\nu}{\tilde{\nu}_1}\right)^{(1-p)/2}\frac{4}{(17p-25)}, \qquad \nu\ge\tilde{\nu}_1,$$

where $Z_1 \equiv Z(m_1)$ and we have used $Z/Z_1 = (\nu_m/\tilde{\nu}_1)^{-4/17}$. We also used the fact that $\tilde{\epsilon}_B^{1/2}$ and m vary slowly with ν_m and took them as constants evaluated at $\nu_m = \tilde{\nu}_1$ where the integral peaks.

For $\nu < \tilde{\nu}_1$ the integral can be written as a sum of two integrals over $\nu_m < \nu$ and $\nu_m > \nu$. Both integrals peak at $\nu_m = \nu$. We denote $m_* = m(\nu_m = \nu)$, $Z_* = Z(m_*)$, and $\tilde{\epsilon}_{B*} = \tilde{\epsilon}_B(m_*)$, use $Z/Z_* = (\nu_m/\nu)^{-4/17}$, and get

$$L_\nu^{\pm}(\nu,\ \tilde{R}) = w(\tilde{R})\frac{k}{2}\tilde{\epsilon}_{B*}^{1/2}\frac{Z_*}{\mu_e}m_*\left\{\frac{4}{17p-25}+\frac{6}{29}\left[1-\left(\frac{\nu}{\tilde{\nu}_1}\right)^{29/51}\right]\right\}, \qquad \nu \le \tilde{\nu}_1. \tag{A12}$$

We used again the slow variation of m and $\tilde{\epsilon}_B$ with ν_m and replaced m by m_* and $\tilde{\epsilon}_B$ by $\tilde{\epsilon}_{B*}$.

A2. $\tilde{R} \ge R_{\rm acc}$

At radii $\tilde{R} > R_{\rm acc}$, the blast wave material has shells with mass coordinate $0 < m < m_{\rm acc}$ and $m_{\rm acc} < m < \tilde{m}$. The $L_\nu^{\pm}$ integral is taken over $0 < m < m_1 = \min\{\tilde{m},\ m_{\rm load}\}$.

For $\nu > \tilde{\nu}_1$ the integral is given by

$$L_\nu^{\pm}(\nu,\ \tilde{R}) = w(\tilde{R})\int_0^{\tilde{\nu}_1}\tilde{\epsilon}_B^{1/2}\frac{Z}{\mu_e}\left(\frac{\nu_m}{\nu}\right)^{(p-1)/2}\frac{k}{2}\left\{\begin{array}{ll}\dfrac{\xi_{\rm acc}}{10\xi} & m > m_{\rm acc}\\ \dfrac{2}{17} & m < m_{\rm acc}\end{array}\right\}m\frac{d\nu_m}{\nu_m}. \tag{A13}$$

Let us denote

$$\tilde{\nu}_{\rm acc}(\tilde{R}) \equiv \nu_m(m_{\rm acc},\ \tilde{R}). \tag{A14}$$

We have $Z \propto \nu_m^{-4/17}$ at $\nu_m < \tilde{\nu}_{\rm acc}$ and $Z \propto \nu_m^{-1/2}$ at $\nu_m > \tilde{\nu}_{\rm acc}$. It is convenient to calculate the integral as a sum of two integrals over $\nu_m < \tilde{\nu}_{\rm acc}$ and $\nu_m > \tilde{\nu}_{\rm acc}$. The first integral peaks at $\nu_m = \tilde{\nu}_{\rm acc}$ and the second at $\nu_m = \tilde{\nu}_1$. We then find

$$\begin{aligned}L_\nu^{\pm}(\nu,\ \tilde{R}) = w(\tilde{R})\frac{k}{2}\left(\frac{\nu}{\tilde{\nu}_1}\right)^{(1-p)/2}\Bigg\{&\tilde{\epsilon}_{B\rm acc}^{1/2}\frac{Z_{\rm acc}}{\mu_e}m_{\rm acc}\frac{4}{17p-25}\left(\frac{\tilde{\nu}_{\rm acc}}{\tilde{\nu}_1}\right)^{(p-1)/2}\\ &+\tilde{\epsilon}_{B1}^{1/2}\frac{Z_1}{\mu_e}m_1\frac{\xi_{\rm acc}}{5(p-2)\xi_1}\left[1-\left(\frac{\tilde{\nu}_{\rm acc}}{\tilde{\nu}_1}\right)^{(p-2)/2}\right]\Bigg\}, \qquad \nu \ge \tilde{\nu}_1,\end{aligned} \tag{A15}$$

where $Z_{\rm acc} \equiv Z(m_{\rm acc}) = 74\mu_e$, $\tilde{\epsilon}_{B\rm acc} \equiv \epsilon_B(m_{\rm acc},\ \tilde{R})$, and $\tilde{\epsilon}_{B1} \equiv \epsilon_B(m_1,\ \tilde{R})$. As soon as the blast wave radius exceeds $R_{\rm acc}$, we have almost immediately $\tilde{\nu}_{\rm acc} \ll \tilde{\nu}_1$ (The frequency $\tilde{\nu}_1$ increases exponentially with $\tilde{R}$ between $R_{\rm acc}$ and $R_{\rm load}$.) Then the terms with $\tilde{\nu}_{\rm acc}/\tilde{\nu}_1$ can be neglected. (These terms are needed only to match smoothly the formula with the results obtained at $\tilde{R} < R_{\rm acc}$.)

Next, consider intermediate ν in the range $\tilde{\nu}_{\rm acc} < \nu < \tilde{\nu}_1$. Then the integral is calculated as a sum of three integrals over $0 < \nu_m < \tilde{\nu}_{\rm acc}$, $\tilde{\nu}_{\rm acc} < \nu_m < \nu$, and $\nu < \nu_m < \tilde{\nu}_1$. In the first interval we use $Z/Z_{\rm acc} = (\nu_m/\tilde{\nu}_{\rm acc})^{-4/17}$, and in the other two intervals $Z/Z_* = (\nu_m/\nu)^{-1/2}$, where the asterisk refers to the point $\nu_m = \nu$. We thus get

$$\begin{aligned}L_\nu^{\pm}(\nu,\ \tilde{R}) = w(\tilde{R})\frac{k}{2}\Bigg\{&\frac{Z_{\rm acc}}{\mu_e}\tilde{\epsilon}_{B\rm acc}^{1/2}m_{\rm acc}\frac{4}{17p-25}\left(\frac{\tilde{\nu}_{\rm acc}}{\nu}\right)^{(p-1)/2}+\frac{Z_*}{\mu_e}\tilde{\epsilon}_{B*}^{1/2}m_*\frac{\xi_{\rm acc}}{\xi_*}\frac{1}{5(p-2)}\left[1-\left(\frac{\tilde{\nu}_{\rm acc}}{\nu}\right)^{(p-2)/2}\right]\\ &+\frac{Z_*}{\mu_e}\tilde{\epsilon}_{B*}^{1/2}m_*\frac{\xi_{\rm acc}}{\xi_*}\frac{3}{25}\left[1-\left(\frac{\nu}{\tilde{\nu}_1}\right)^{5/6}\right]\Bigg\}, \qquad \tilde{\nu}_{\rm acc} \le \nu \le \tilde{\nu}_1.\end{aligned} \tag{A16}$$

Finally, at low $\nu < \tilde{\nu}_{\rm acc}$, the integral is calculated as a sum of three integrals over $0 < \nu_m < \nu, \nu < \nu_m < \tilde{\nu}_{\rm acc}$, and $\tilde{\nu}_{\rm acc} < \nu_m < \tilde{\nu}_1$. In the first two intervals we use $Z/Z_* = (\nu_m/\nu)^{-4/17}$, and in the last interval $Z/Z_{\rm acc} = (\nu_m/\tilde{\nu}_{\rm acc})^{-1/2}$,

$$\begin{aligned}L_\nu^{\pm}(\nu,\ \tilde{R}) = w(\tilde{R})\frac{k}{2}\Bigg\{&\frac{Z_*}{\mu_e}\tilde{\epsilon}_{B*}^{1/2}m_*\frac{4}{17p-25}+\frac{Z_*}{\mu_e}\tilde{\epsilon}_{B*}^{1/2}m_*\frac{6}{29}\left[1-\left(\frac{\nu}{\tilde{\nu}_{\rm acc}}\right)^{29/51}\right]\\ &+\frac{Z_{\rm acc}}{\mu_e}\tilde{\epsilon}_{B\rm acc}^{1/2}m_{\rm acc}\frac{3}{25}\left(\frac{\nu}{\tilde{\nu}_{\rm acc}}\right)^{1/3}\left[1-\left(\frac{\tilde{\nu}_{\rm acc}}{\tilde{\nu}_1}\right)^{5/6}\right]\Bigg\}, \qquad \nu \le \tilde{\nu}_{\rm acc}.\end{aligned} \tag{A17}$$

A3. Z_* AND m_*

The above formulae for $L_\nu^\pm$ should be made explicit by expressing m_*, ξ_*, and Z_* in terms of ν and $\tilde{R}$.

Equation (A11) gives $Z(\nu_m)$, and we get $Z = Z_*$ at $\nu_m = \nu$,

$$\frac{Z_*}{\mu_e} = \begin{cases} \left[\nu(1+\beta_*)^{3/2} n_{0*}^{1/2} q^{-1} \tilde{\epsilon}_{B*}^{-1/2} \Gamma_*^{-1}\right]^{-1/2}, & m_* > m_{\rm acc}, \\ \left[\nu(1+\beta_*)^{3/2} n_{0*}^{1/2} q^{-1} \tilde{\epsilon}_{B*}^{-1/2} \Gamma_*^{-1}\right]^{-4/17} 74^{9/17}, & m_* < m_{\rm acc}. \end{cases} \tag{A18}$$

All quantities with asterisks are taken at $R = R_*$ ($\nu_m = \nu$). Since R_* is very close to $R_{\rm acc}$ (see eq. [A23]), it is sufficient to use the first approximation $R_* = R_{\rm acc}$ in the equation for Z_*. Then we get

$$\frac{Z_*}{\mu_e} = \begin{cases} \Phi, & 1 < \Phi < 74, \\ 74\left(\dfrac{\Phi}{74}\right)^{8/17}, & \Phi > 74, \end{cases} \tag{A19}$$

where

$$\Phi\left(\nu,\ \tilde{R}\right) = \left(\frac{\nu n_{0\rm acc}^{1/2}}{q \tilde{\epsilon}_{B\rm acc}^{1/2} \Gamma_{\rm acc}}\right)^{-1/2}, \tag{A20}$$

and the subscript "acc" marks that the quantity is taken at $m = m_{\rm acc}$.

Note that

$$\Phi = 74\left(\frac{\nu}{\tilde{\nu}_{\rm acc}}\right)^{-1/2} \tag{A21}$$

at $\tilde{R} \geq R_{\rm acc}$.

The relation between ξ and Z is given by equation (4), and we find ξ_*,

$$\frac{\xi_*}{\xi_{\rm acc}} = \begin{cases} \dfrac{1}{5} \ln\left(\Phi + \sqrt{\Phi^2 - 1}\right), & 1 < \Phi < 74, \\ \left(\dfrac{\Phi}{74}\right)^{4/17}, & 74 < \Phi < 8\times 10^3. \end{cases} \tag{A22}$$

(Here $\Phi = 8\times 10^3$ corresponds to $\xi_* = 3\xi_{\rm acc}$.) Using the relation between R and ξ (eq. [3]), we get

$$\frac{R_*}{R_{\rm acc}} = \begin{cases} \left[\dfrac{1}{5} \ln(2\Phi)\right]^{-1/2}, & 1 < \Phi < 74, \\ \left(\dfrac{\Phi}{74}\right)^{-2/17}, & 74 < \Phi < 8\times 10^3, \end{cases} \tag{A23}$$

where we took $\Phi + (\Phi^2 - 1)^{1/2} \approx 2\Phi$. The corresponding m_* is

$$\frac{m_*}{m_{\rm acc}} = \left(\frac{R_*}{R_{\rm acc}}\right)^k = \left(\frac{\xi_*}{\xi_{\rm acc}}\right)^{-k/2}. \tag{A24}$$

A4. FINAL RESULT

The terms with $\tilde{\epsilon}_{B\rm acc}^{1/2}$ are nonnegligible when $\nu \sim \nu_{\rm acc}$ and $m_* \approx m_{\rm acc}$; therefore, one can replace $\tilde{\epsilon}_{B\rm acc}^{1/2}$ by $\tilde{\epsilon}_{B*}^{1/2}$ and simplify the derived expressions. The final result is as follows:

$$L_\nu^\pm\left(\nu,\ \tilde{R}\right) = 30\left[\frac{\tilde{n}_0}{\mu_e \tilde{\gamma}\left(1+\tilde{\beta}\right)}\right]^{1/2} \begin{cases} Q_* m_* Z_* \tilde{\epsilon}_{B*}^{1/2}, & \nu \leq \tilde{\nu}_1, \\ Q_1 m_1 Z_1 \epsilon_B^{1/2} \left(\dfrac{\nu}{\tilde{\nu}_1}\right)^{(1-p)/2}, & \nu \geq \tilde{\nu}_1, \end{cases} \tag{A25}$$

$$Q_*(\nu,\ \tilde{R}) = \frac{k}{2}\left\{\frac{4}{17p-25}+\frac{6}{29}\left[1-\left(\frac{\nu}{\tilde{\nu}_1}\right)^{29/51}\right]\right\}, \qquad \tilde{R} \le R_{\rm acc}, \tag{A26}$$

$$Q_*(\nu,\ \tilde{R}) = \frac{k}{2}\left\{\frac{(3p-1)}{25(p-2)}\frac{\xi_{\rm acc}}{\xi_*}+\left(\frac{\tilde{\nu}_{\rm acc}}{\nu}\right)^{(p-1)/2}\left[\frac{4}{17p-25}\frac{m_{\rm acc}}{m_*}-\frac{1}{5(p-2)}\frac{\xi_{\rm acc}}{\xi_*}\right]-\left(\frac{\nu}{\tilde{\nu}_1}\right)^{5/6}\frac{3}{25}\frac{\xi_{\rm acc}}{\xi_*}\right\}, \quad \tilde{R} \ge R_{\rm acc}, \quad \tilde{\nu}_{\rm acc} \le \nu \le \tilde{\nu}_1, \tag{A27}$$

$$Q_*(\nu,\ \tilde{R}) = \frac{k}{2}\left\{\frac{4}{17p-25}+\frac{6}{29}+\left(\frac{\nu}{\tilde{\nu}_{\rm acc}}\right)^{29/51}\left(\frac{3}{25}\frac{m_{\rm acc}}{m_*}-\frac{6}{29}\right)-\frac{3}{25}\frac{m_{\rm acc}}{m_*}\left(\frac{\nu}{\tilde{\nu}_{\rm acc}}\right)^{29/51}\left(\frac{\tilde{\nu}_{\rm acc}}{\tilde{\nu}_1}\right)^{5/6}\right\}, \quad \tilde{R} \ge R_{\rm acc}, \quad \nu \le \tilde{\nu}_{\rm acc} \le \tilde{\nu}_1, \tag{A28}$$

$$Q_1(\nu,\ \tilde{R}) = \frac{k}{2}\frac{4}{17p-25}, \qquad \tilde{R} \le R_{\rm acc}, \tag{A29}$$

$$Q_1(\nu,\ \tilde{R}) = \frac{k}{2}\left\{\frac{1}{2(p-1)}\frac{\xi_{\rm acc}}{\xi_1}+\left(\frac{\tilde{\nu}_{\rm acc}}{\tilde{\nu}_1}\right)^{p/2-1}\left[\frac{4}{17p-25}\frac{m_{\rm acc}}{m_1}-\frac{1}{2(p-1)}\frac{\xi_{\rm acc}}{\xi_1}\right]\right\}, \qquad \tilde{R} \ge R_{\rm acc}. \tag{A30}$$

The ratios $\xi_*/\xi_{\rm acc}$ and $m_*/m_{\rm acc}$ appearing in the expressions for Q_* at $\tilde{R} > R_{\rm acc}$ are given by

$$\left(\frac{m_*}{m_{\rm acc}}\right)^{-s/k} = \frac{\xi_*}{\xi_{\rm acc}} = \begin{cases} 1-0.1\ln\left(\dfrac{\nu}{\tilde{\nu}_{\rm acc}}\right), & \nu \ge \tilde{\nu}_{\rm acc}, \\ \left(\dfrac{\nu}{\tilde{\nu}_{\rm acc}}\right)^{-2/17}, & \nu \le \tilde{\nu}_{\rm acc}. \end{cases} \tag{A31}$$

In this paper we are interested in $\tilde{R} > R_{\rm acc}$ and $\nu < \tilde{\nu}_1$. Then

$$L_\nu^{\pm} = 30(\tilde{\epsilon}_{B*}\tilde{n}_0)^{1/2}Q_* m_* Z_*, \tag{A32}$$

and the numerical factor f_ν defined in equation (67) is given by

$$f_\nu = Q_*\frac{m_* Z_*}{m_{\rm acc}Z_{\rm acc}}\left(\frac{\tilde{\epsilon}_{B*}}{\tilde{\epsilon}_{B\rm acc}}\right)^{1/2}. \tag{A33}$$

This factor is shown in Figure 9 assuming $\tilde{\epsilon}_{B*} = \tilde{\epsilon}_{B\rm acc}$.

REFERENCES

Akerlof, C., et al. 1999, Nature, 398, 400
Beloborodov, A. M. 2002, ApJ, 565, 808 (B02)
———. 2003a, ApJ, 585, L19
———. 2003b, ApJ, 588, 931
———. 2005, ApJ, 618, L13
Blandford, R. D., & McKee, C. F. 1976, Phys. Fluids, 19, 1130
Derishev, E. V., Kocharovsky, V. V., & Kocharovsky, Vl. V. 1999, ApJ, 521, 640
Fan, Y. Z., Zhang, B., & Wei, D. M. 2004, ApJ, submitted (astro-ph/0412105)
Granot, J., Piran, T., & Sari, R. 1999, ApJ, 527, 236
Kumar, P., & Panaitescu, A. 2004, MNRAS, 354, 252
Li, Z., Dai, Z. G., & Lu, T. 2003, MNRAS, 345, 1236
Madau, P., & Thompson, C. 2000, ApJ, 534, 239
Medvedev, M. M., & Loeb, A. 1999, ApJ, 526, 697
Mészáros, P., Ramirez-Ruiz, E., & Rees, M. J. 2001, ApJ, 554, 660
Mészáros, P., & Rees, M. J. 1993, ApJ, 418, L59
Panaitescu, A., & Kumar, P. 2000, ApJ, 543, 66
———. 2002, ApJ, 571, 779
Peng, F., Königl, A., & Granot, J. 2004, ApJ, submitted (astro-ph/0410384)
Piran, T. 2004, Rev. Mod. Phys., 76, 1143
Preece, R. D., et al. 2000, ApJS, 126, 19
Rybicki, G. B., & Lightman, A. P. 1979, Radiative Processes in Astrophysics (New York: Wiley)
Sari, R., & Esin, A. A. 2001, ApJ, 548, 787
Sari, R., & Piran, T. 1999, ApJ, 517, L109
Sari, R., Piran, T., & Narayan, R. 1998, ApJ, 497, L17
Stern, B. E. 2003, MNRAS, 345, 590
Thompson, C., & Madau, P. 2000, ApJ, 538, 105